

Unifying warfighting functions in mathematical modelling: combat, manoeuvre, and C2

Ryan Ahern^a, Mathew Zuparic^b, Keeley Hoek^c and Alexander Kalloniatis^b

^a Monash University, Clayton, VIC, Australia; ^b Defence Science and Technology Group, Canberra, ACT, Australia; ^c Australian National University, Canberra, Australia.

ARTICLE HISTORY

Compiled January 25, 2023

ABSTRACT

The outcomes of warfare have rarely only been characterised by the quantity and quality of individual combatant force elements. The ability to manoeuvre and adapt across force elements through effective Command and Control (C2) can allow smaller or weaker forces to overcome an adversary with greater resource and fire-power. In this paper, we combine the classic Lanchester combat model with the Kuramoto-Sakaguchi model for phase oscillators on a network to create a flexible Networked-Lanchester-C2 representation of force-on-force military engagement. The mathematical model thus unifies three of the military warfighting ‘functions’: fires, manoeuvre and C2. We consider three illustrative use-cases, and show that an analytical treatment of a reduced model characterises global effects in the full system. For inhomogeneous forces we observe that with appropriate balance between internal organisational coupling, resource manoeuvrability and even weaker lethality the force can be adaptive to overcome an initially stronger adversary.

KEYWORDS

Lanchester, command and control, manoeuvre, synchronisation

1. Introduction

Since the dawn of organised warfare, strategy and tactics have enabled commanders to defeat numerically superior foes. In particular, the ability to outmanoeuvre the forces of an opponent can open opportunities for a more decisive result than purely attritional warfare. We propose to mathematically model these dynamics through coupled differential equations, integrating combat, manoeuvre, and Command and Control (C2).

Napoleon is arguably the most famous, and defining, example of superior manoeuvrability of forces at a *campaign* level (Van Creveld, 1985), able to shift his forces between distributed and then concentrated at a decisive point, with synchronisation a key enabler for his victories. There are also *more localised* examples where a cleverly diffuse, agile and responsive force has been able to defeat a numerically superior opponent. At the battle of Cynoscephalae in 197 BC (Polybius, 1927), the superior manoeuvrability and controllability of the *maniple* tactical sub-division formation enabled Roman victory over the Macedonian *phalanx* and heavy cavalry. At the battle of Crécy (Reid, 2007) in 1346, with the introduction of the English longbow, tactics were enabled to effectively disrupt the (usually devastating) heavy cavalry charge so that the English defeated a vastly numerically superior French army. Manoeuvre ideas

were again vindicated with the Blitzkrieg of the German Wehrmacht in World War II, and coalition forces in the First Gulf War.

The model we propose builds upon the Lanchester square (directed-fire) model (Lanchester, 1916),

$$\dot{p}_B = -\alpha_{RB}p_R, \quad p_B = p_{B0} \text{ when } t = 0, \quad \dot{p}_R = -\alpha_{BR}p_B, \quad p_R = p_{R0} \text{ when } t = 0, \quad (1)$$

where α_{RB}, α_{BR} give the combat effectiveness, or lethality, for the Red and Blue force, respectively, and p_R, p_B are the resource *populations* of Red and Blue respectively. As a constant coefficient linear system of ordinary differential equations a conserved quantity from Eq.(1) is analytically solvable, meaning that lethalties and initial resources determine the outcome of the battle.

Note that other models lack continuous battle dynamics, as in the Colonel Blotto game (Roberson, 2006), or the Hughes salvo model (Hughes, 1995) of naval warfare. The Lanchester model has been extended to fit empirical data in different historical contexts (Bracken, 1995) (see also (Fricker, 1998) and (Lucas & Turkes, 2004)), has been extended to the more recent *mixed forces* variant by (MacKay, 2009) and (Kress *et al.*, 2018), has been used for *artificial intelligence* playing the real-time-strategy game *Starcraft* (Stanescu *et al.*, 2015) and for asymmetric guerilla warfare with (Deitchman, 1962) and (Schaffer, 1968).

In all these, the functions of command and manoeuvre are buried in the combat effectiveness *constant*. This is reasonable when fitting against data for two forces with unchanged strategy over a drawn out engagement, but this is rarely true even for simple social animals, as discussed in (Adams & Mesterton-Gibbons, 2003) and (Plowes & Adams, 2005). It is also difficult to estimate *a priori* the combat effectiveness for a force, or assess the stability of the effectiveness to changes in organisation. More significantly, the role of information and communication technology in enabling the organisation of diverse (for example, from different military services) elements of a force has made the *network* paradigm potent for contemporary and future warfare. This has led, in recent decades, to the proposition of what was coined as ‘Network Centric Warfare’ (Alberts *et al.*, 1999) linking network connectivity, self-synchronisation of force elements and effective military outcomes. Though the Lanchester model has been treated as an abstraction for network *cyber* attack and defence (Liu *et al.*, 2013), a model with explicit network structure was only proposed in (Kalloniatis *et al.*, 2020a) by generalising MacKay’s (MacKay, 2009) mixed-forces model. Here network optimisation led to identification of concepts in the Manoeuvre Theory of Warfare.

In this paper we bring C2 into the formulation of (Kalloniatis *et al.*, 2020a) using the Kuramoto-Sakaguchi (Sakaguchi & Kuramoto, 1986) model of phase oscillators (which builds on (Kuramoto, 1984)), thereby unifying three key warfighting functions, C2, Manoeuvre and Fires in a single mathematical model. For general networks, as developed by (Acebrón *et al.*, 2005), (Arenas *et al.*, 2008), (Dörfler & Bullo, 2014) and (Rodrigues *et al.*, 2016) the model is

$$\dot{\theta}_i = \omega_i - \sum_{j \in \mathcal{K}} \sigma_{ij} \mathcal{K}_{ij} \sin(\theta_i - \theta_j - \Phi_{ij}), \quad i \in \mathcal{K}, \quad (2)$$

where for the i th node, $\theta_i \in \mathbb{S}^1$ is the phase, $\omega_i \in \mathbb{R}$ is the natural frequency, $\sigma_{ij} \in \mathbb{R}_+$ is the coupling strength on node i from node j , \mathcal{K} is the adjacency matrix representing the network, and $\Phi_{ij} \in \mathbb{S}^1$ represents a ‘frustration’ between node i and j , where phase θ_i attempts to stay amount Φ_{ij} ahead of phase θ_j . It is well-known that at sufficiently

high couplings σ_{ij} , phases approximately align $\theta_i(t) \approx \theta_j(t)$ and synchronise to (for undirected graphs) the mean of the natural frequencies $\bar{\omega}$.

For application to C2 (Kalloniatis *et al.*, 2020b), the phases represent decision cycles of individual agents, the natural frequencies the decision speeds of agents if left to themselves, coupling strengths represent the tightness of relationship (or responsiveness to changes in decision state) between agents, the network represents the formal and informal organisational C2 structure, and the frustrations represent how far ahead agents *seek* to be in relation to other agents. The same framework of Eq.(2) can be extended to two (or more (Zuparic *et al.*, 2021)) forces or populations in competition with each other. Two elements quantified here mathematically are well documented as *qualitative* properties of decision-making and organisations: the cyclicity of individual decision-making, in the Perception-Action cycle of cognitive psychology (Neisser, 1976) or the Observe-Orient-Decide-Act (OODA) loop of military and business strategy (Osinga, 2006); and the role of loose and tight coupling in organisations as articulated by (Weick, 1976), (Perrow, 2011) and (Hollenbeck & Spitzmueller, 2012). This model thus brings long articulated ideas in organisational theory into a dynamical mathematical model.

To illustrate these ideas more specifically in terms of the variables we have introduced consider that the first N components of θ_i represent the decision state in a continuous version of the OODA loop for individual Blue members of the Blue C2 system or network. The remaining M components represent the (OODA) decision state of Red agents within their own corresponding C2 system. In the spirit of Boyd’s admonition each of Blue and Red will seek to stabilise their decision state ahead of each other, $\phi_i > \phi_j$ where i, j may represent Blue or Red. Thus each side aims for locking a certain phase shift ahead of the other: Φ_{BR} for Blue in relation to Red, and Φ_{RB} for Red with respect to Blue; for simplicity here we treat the frustration values homogeneously within each group, Blue or Red. These frustration values represent a target state for each side. Whether they achieve that depends on the dynamics represented in Eq. 2, subject to their couplings, their connectivity, and their individual capacity for rapid decision making.

Till now, the ‘decisions’ referred to have been in the abstract. In this paper we wed this to what C2 is meant to accomplish in a military force. Thus we model the situation that if one of Blue or Red have their phase θ_i ahead of the other, θ_j they will gain an advantage in the Lanchester dynamics. We thus propose a mathematical model naturally unifying the combat, manoeuvre and C2 warfighting functions using a multi-layer network formulation (Boccaletti *et al.*, 2014). The model is more compact than an alternative contemporary equation-based approach by (McLemore *et al.*, 2016), noting that they spatially embed force elements and omit C2.

For homogeneous forces our unified model can be simplified to a global form, with which we start to illustrate the construction, and build on a use-case from experience with the Kuramoto-Sakaguchi model (Kalloniatis & Zuparic, 2016). Though not solvable, the global model permits considerable dimensional reduction and insight. When inhomogeneity is high the global model is more limited, but the full model demonstrates *adaptive* dynamics where one force, say Blue, must change its resource distribution to adjust for a stronger Red force. Finally, with a fictitious complex network we illustrate how the complete model may be used in a classic Operational Research sense, to investigate trade-offs between investment in fire-power or C2 systems.

In the following, we present the principles of the model by showing how C2 and combat dynamics may be combined in a unified Lanchester-Kuramoto-Sakaguchi model. We examine this model only insofar as it builds an intuition and approximation

scheme that can be applied to the full model. We then formulate the fully networked Lanchester-Kuramoto-Sakaguchi model and consider it for the first two use-cases, followed by a complex network to show the utility of the networked model in Operational Research. We conclude and discuss future developments. Further details of analytical calculations and examination of a use-case are relegated to the Appendix.

2. Unifying the Lanchester equations with the Kuramoto-Sakaguchi model

In the following we first outline the adversarial form of the Kuramoto-Sakaguchi model before then showing it may be unified with the Lanchester equations and then analysing to some degree the properties of the model. We emphasise that this is both to establish the principles of how we develop the more advanced model later on, and establish some intuition into its behaviours to provide a foundation for analysing the fully networked model in Sec.3. We provide two cases of such a model, one where the C2 impacts on the Lanchester dynamics unilaterally, and the other where attrition can in turn degrade the ability of a force to undertake its decision making. We examine how far a semi-analytical approach can go in understanding behaviours detected in numerical solutions.

2.1. Adversarial form of Kuramoto-Sakaguchi model

To begin with we show how Eq.(2) may be written to distinguish two adversary forces that we call the ‘Blue-Red’ formulation (Kalloniatis & Zuparic, 2016). We adopt here a more compact formulation compared to that work with the following block matrix variable form for coupling, frustration and network structures:

$$\sigma = \begin{bmatrix} \sigma_B & \zeta_{BR} \\ \zeta_{RB} & \sigma_R \end{bmatrix}, \quad \Phi = \begin{bmatrix} 0 & \phi^{BR} \\ \phi^{RB} & 0 \end{bmatrix}, \quad \mathcal{K} = \begin{bmatrix} \mathcal{B} & \mathcal{A}^{BR} \\ \mathcal{A}^{RB} & \mathcal{R} \end{bmatrix}. \quad (3)$$

The blocks in σ and Φ have the same dimension as those in \mathcal{K} so that diagonal unit matrices are implicit in the respective blocks, while θ becomes a vector composed of two blocks of dimension $|\mathcal{B}|$ and $|\mathcal{R}|$ for the number of Blue and Red agents, respectively. Here ζ denotes an inter-network coupling, \mathcal{A} matrices encode any inter-network edges and the frustration ϕ is set to zero for intra-network connections — though this condition can be relaxed in future. In this notation ζ_{BR} represents Red’s coupling to Blue, ϕ^{BR} the degree to which Red seeks to be ahead of Blue’s phase and \mathcal{A}^{BR} the structure of Red’s interactions with Blue; reversing the labels B and R gives Blue’s pattern of engagement with Red. We thus capture a distinction between internal processes of a force, Blue or Red, from their interactions with each other. In particular, the vanishing diagonals, and taking $\{\phi^{BR}, \phi^{RB}\} > 0$ means that Blue and Red seek to internally synchronise their decision-cycles while trying to be ahead of each others cycles. Such multi-network models (Boccaletti *et al.*, 2014) exhibit collective synchronisation effects that motivate their use in a C2-enabled Lanchester model.

In this paper, local synchronisation denotes the extent to which all nodes of a particular sub-network are phase-locked, i.e. $\theta_i = \theta_j \forall i, j \in \mathcal{B}$ or \mathcal{R} describes a phase-locked Blue or Red sub-network. (If $\theta_i = \theta_j$ for all nodes across the combined Blue-Red system then we may speak of global synchronisation.) We may quantify this

by sampling the instantaneous agreement in phase, referred to as the ‘order parameter’

$$O_B(t) \equiv \frac{\left| \sum_{j \in \mathcal{B}} e^{\sqrt{-1}\theta_j(t)} \right|}{|\mathcal{B}|}, \quad O_R(t) \equiv \frac{\left| \sum_{j \in \mathcal{R}} e^{\sqrt{-1}\theta_j(t)} \right|}{|\mathcal{R}|}. \quad (4)$$

Note here we explicitly use the imaginary unit $\sqrt{-1}$ rather than the oft-used symbol i because of the prevalence of the latter as an index for graph structure. Also, factors such as $\sum_{j \in \mathcal{B}} e^{\sqrt{-1}\theta_j(t)}$ are easily seen to amount to the cosine of difference of phases through multiplication by the complex conjugate and symmetry considerations. Thus, the range of O , for either Blue or Red, is seen to be between zero and unity inclusive, where $O = 1$ is attained if the phase of all nodes coincide (zero phase difference) and $O = 0$ if the node phases are randomly distributed uniformly around the decision circle. Thus, the order parameter allows us to represent force cohesion and include this effect in the organisational component of force effectiveness.

2.2. Unifying Lanchester and Kuramoto: C2 as Force Multiplier

The key to unifying the two dynamical modelling paradigms is the notion that C2 can be a *force-multiplier*, namely a factor that makes a set of weapons act as more than just the sum of their individual strengths. Thus, in this paper, we assume that force effectiveness in Lanchester is *multiplicatively separable* into *physical* κ and *organisational* Ω components, and apply the Kuramoto-Sakaguchi (Sakaguchi & Kuramoto, 1986) model as a framework to introduce organisational decision-making type dynamics. Hence, each lethality coefficient is factored as

$$\alpha_{BR} = \kappa_{BR} \cdot \Omega_{BR}, \quad \alpha_{RB} = \kappa_{RB} \cdot \Omega_{RB}. \quad (5)$$

For the time being, we keep the physical effects $\kappa \in \mathbb{R}_+$ as a constant positive variable, but generate the organisational effects Ω dynamically, $\Omega = \Omega(t)$. These effects are achieved via the Red-Blue Kuramoto-Sakaguchi model originally considered in (Kalloniatis & Zuparic, 2016)

$$\begin{aligned} \dot{\theta}_i^B &= \omega_i^B - \sigma_B \sum_{j \in \mathcal{B}} \mathcal{B}_{ij} \sin(\theta_i^B - \theta_j^B) - \zeta_{BR} \sum_{j \in \mathcal{R}} \mathcal{A}_{ij}^{BR} \sin(\theta_i^B - \theta_j^R - \phi^{BR}), \quad i \in \mathcal{B}, \\ \dot{\theta}_i^R &= \omega_i^R - \sigma_R \sum_{j \in \mathcal{R}} \mathcal{R}_{ij} \sin(\theta_i^R - \theta_j^R) - \zeta_{RB} \sum_{j \in \mathcal{B}} \mathcal{A}_{ij}^{RB} \sin(\theta_i^R - \theta_j^B - \phi^{RB}), \quad i \in \mathcal{R} \end{aligned} \quad (6)$$

where θ_i^B and θ_i^R are time-dependent. In the following we seek a form for Ω that captures the advantage provided by a force being collectively ahead of the decision cycle of the adversary.

2.3. Global phases and organisational effect on combat

Because the Lanchester model in Eq.(1) only describes homogeneous forces, we need to extract correspondingly global properties of the adversarial C2 model. To this end we consider the *global phases* (or centroids) for agents in the Blue and Red networks,

denoted by Θ_B and Θ_R , respectively,

$$\Theta_B = \frac{1}{|\mathcal{B}|} \sum_{i \in \mathcal{B}} \theta_i^B, \quad \Theta_R = \frac{1}{|\mathcal{R}|} \sum_{j \in \mathcal{R}} \theta_j^R. \quad (7)$$

The difference between global phases is designated Δ_{BR} :

$$\Delta_{BR} \equiv \Theta_B - \Theta_R = -\Delta_{RB}. \quad (8)$$

Applying the difference of global phases, we consider the following form for the organisational component of Blue/Red force effectiveness against Red/Blue,

$$\Omega_{BR} = O_B \left(\frac{1 + \sin \Delta_{BR}}{2} \right), \quad \Omega_{RB} = O_R \left(\frac{1 + \sin \Delta_{RB}}{2} \right). \quad (9)$$

These Ω consist of the multiplication of two dynamic quantities which vary between zero and unity. Hence, each side gains organisational advantage by maintaining good intra-network synchronisation, *and* staying ahead (maximally $\pi/2$) of their competitor's collective decision phase. Conversely, organisational advantage is lost by the loss of intra-network synchronisation, *and/or* being behind (with a minimum achieved at $-\pi/2$) their competitor's collective decision phase, as depicted in Fig.1. Additionally, the choice of sine (as opposed to tanh) allows decision advantage to be periodic and thus continuous over domain \mathbb{S}^1 . Inserting this into Eq.(5) yields

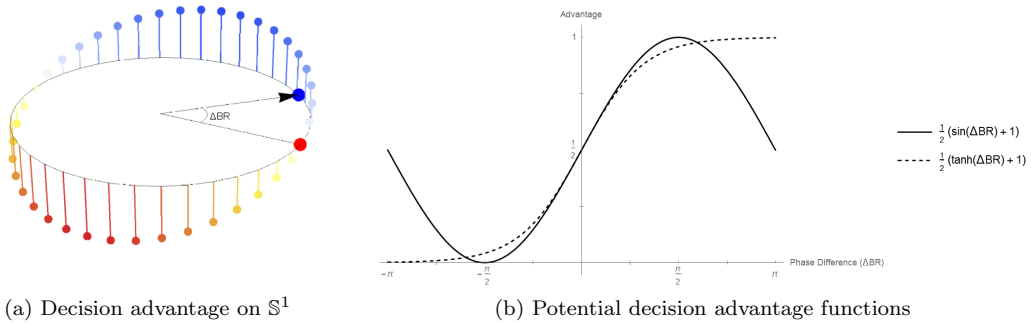


Figure 1.: A three-dimensional perspective of the interpretation of sinusoidal advantage location on the decision circle (a) and a plot of different advantage functions (b). In both cases the Red node/cluster is located at zero angle and the Blue node/cluster is swept through values of Phase Difference Δ_{BR} .

$$\dot{p}_B = -\kappa_{RB} O_R \left(\frac{1 - \sin \Delta_{BR}}{2} \right) p_R \mathcal{H}(p_B), \quad \dot{p}_R = -\kappa_{BR} O_B \left(\frac{1 + \sin \Delta_{BR}}{2} \right) p_B \mathcal{H}(p_R), \quad (10)$$

where in order to avoid the appearance of negative populations, we enforce non-negativity with a Heaviside-step function $\mathcal{H}(x)$. The full generalised C2-Lanchester model is thus Eq.(10), in combination with Eq.(6) representing the dynamics of adversarial organisational decision cycles. We provide a comprehensive list of variables and parameters used to define the Lanchester-Kuramoto-Sakaguchi model in Table 1.

Table 1.: Summary of the Kuramoto-Sakaguchi and Lanchester inspired variables and parameters defined in Sec. 2 and 3, and their physical interpretations.

expression	name	interpretation
$\{\theta^B, \theta^R\}$	phase	agent decision state
$\{\mathcal{B}, \mathcal{R}\}$	adjacency matrix	internal decision-making network
ω^X	natural frequency	decision-speed of \mathcal{X} agent in isolation
σ_X	intra-network coupling	intensity of intra-agent interaction in \mathcal{X}
\mathcal{A}^{XY}	inter-adjacency matrix	topology between \mathcal{X} and \mathcal{Y} decision-makers
ζ_{XY}	inter-network coupling	intensity of \mathcal{X} 's interaction with \mathcal{Y}
ϕ^{XY}	frustration	\mathcal{X} 's strategy against \mathcal{Y} 's decision-makers
O_X	global order parameter	measure of global synchronisation of decision-making agents in \mathcal{X}
O_i^X	local order parameter	measure of local synchronisation of agent i with its nearest neighbours in \mathcal{X}
Θ_X	global phase	average phase of agents in \mathcal{X}
Δ_{XY}	average phase difference	average difference of phases between networks \mathcal{X} and \mathcal{Y}
$\{p^B, p^R\}$	population size	force/resource strength
κ_{XY}	physical effectiveness	efficacy of \mathcal{X} 's physical capabilities applied to \mathcal{Y}
Ω_{XY}	organisational effectiveness	efficacy of \mathcal{X} 's decision-making capabilities applied to \mathcal{Y}
α_{XY}	lethality	\mathcal{X} 's total combat effectiveness against \mathcal{Y}
$\{\mathcal{M}^B, \mathcal{M}^R\}$	manoeuvre networks	internal force-flow network topology
\mathcal{E}^{XY}	engagement network	topology between \mathcal{M}^X and \mathcal{M}^Y
δ	flow moderation	force-networks where combat occurs
d	engagement moderation	dynamic moderation of force transfer
		dynamic moderation of combat outcomes

2.4. Numerical simulation: use-case 1

We now turn to numerical simulation of the model to gain insight into its behaviours. For this purpose we approximate the Heaviside function as follows:

$$\mathcal{H}(x) \approx [1 + \tanh((x - \epsilon_1)/\epsilon_2)]/2 \quad (11)$$

where $\epsilon_1 > \epsilon_2 > 0$ are small. In this paper we numerically solve using Mathematica's NDSolve method, to which end we choose $\epsilon_1 = 10^{-15}$, $\epsilon_2 = 10^{-20}$. Here we consider a use-case of competition between agents organised, respectively, in a hierarchical and a random organisational structures, as in (Holder *et al.*, 2017) where we have already established a thorough understanding of the potential dynamics of the model. These two organisations may be seen as caricatures of the formal chain-of-command of traditional military forces, on the one-hand, and the *ad hoc* nature of, say, many insurgent groups. This simplification is purely for illustrative purposes.

Consider the nearly symmetric scenario of (Kalloniatis & Zuparic, 2016)

$$|\mathcal{B}| = |\mathcal{R}|, \quad \zeta_{BR} = \zeta_{RB}, \quad (12)$$

yet with different internal networks, couplings, frustrations and physical combat effectiveness. The sub-network structures themselves take the form described in Fig.2 with Blue a hierarchy defined by a complete 4-ary tree such that $N_B = 21$ and Red a random Erdős-Rényi network with an edge probability of 0.4 between the same number $N_R = 21$ nodes. For the adversarial engagement between Blue and Red, we take that one each of the leaf nodes of Blue (the tree, labelled $6, \dots, 21$) engages with a correspondingly indexed member of Red.

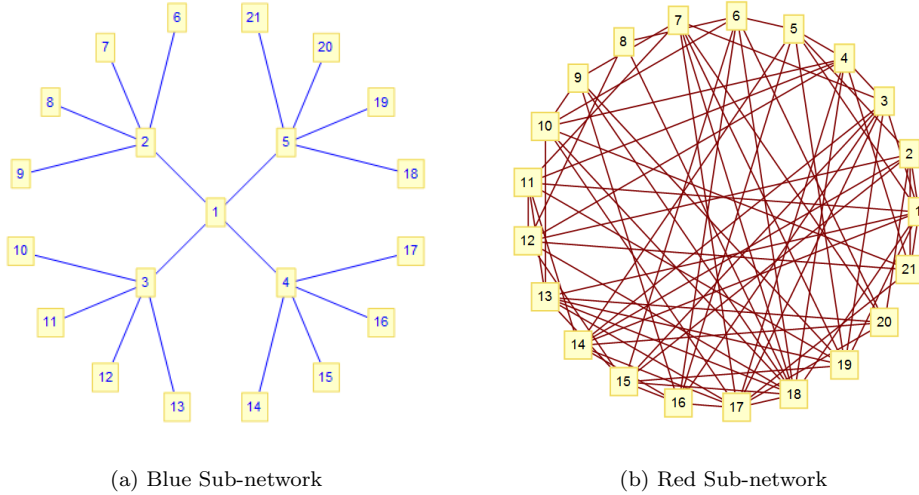


Figure 2.: A graphical depiction of the sub-network structure for each force in use-case 1. The first five nodes, labelled 1-5, have no inter-network connections. All other nodes, labelled 6-21, are connected to the identically labelled node in the opposing network.

We choose internal couplings $\sigma_B = 8$, $\sigma_R = 0.5$ sufficiently large that each network achieves internal synchronisation when considered separately. Again, this crudely represents the property that traditional military hierarchies also apply strong discipline and training to achieve tight interaction between members, while *ad hoc* organisations are much ‘looser’ affairs. That such couplings are necessary for the respective structures to achieve internal coherence is confirmation that the Kuramoto model captures aspects of real world C2 dynamics. Note that, even though this appears to negate the difference between the Blue and Red we shall see that the higher connectivity of the latter leaves its imprint in many of the results.

We also set $\zeta_{BR} = \zeta_{RB} = 0.4$, $\kappa_{BR} = \kappa_{RB} = 0.005$, and randomly select the natural frequencies from a uniform distribution $[0, 1]$. The particular choice we have worked with in (Kalloniatis & Zuparic, 2016) has $\bar{\omega}_R = 0.551$, $\bar{\omega}_B = 0.503$, where $\bar{\omega}_B$ and $\bar{\omega}_R$ are the mean of the Blue and Red natural frequencies respectively. This small difference in means means that in the absence of inter-network interactions Red would slowly lap Blue. Typically, random initial conditions are chosen for numerical calculations which typically thermalise in pure Kuramoto dynamics. However, in view of the role that initial conditions play in the Lanchester model, as in its conservation laws, we choose an unconventional set of initial conditions here to minimise *random* advantages to one side or the other. We choose the phases of all nodes to be initially equi-spaced in the circular sector enclosed by $[-\frac{\pi}{4}, \frac{\pi}{4}]$, i.e. $\theta_{0,j}^B = \theta_{0,j}^R = -\frac{\pi}{4} + \frac{\pi}{2} \frac{j-1}{|\mathcal{B}|-1}$ where $i = 1, 2, \dots, |\mathcal{B}|$. The starting population for each side is equal $p_B|_{t=0} = p_{B0} = p_R|_{t=0} = p_{R0} = 2100$.

The system is solved numerically by Mathematica’s NDSolve until $t_{final} = 10^4$, at which point the difference combat populations

$$p_{final} = p_B|_{t=t_{final}} - p_R|_{t=t_{final}} \quad (13)$$

is recorded, as shown in Fig. 3.

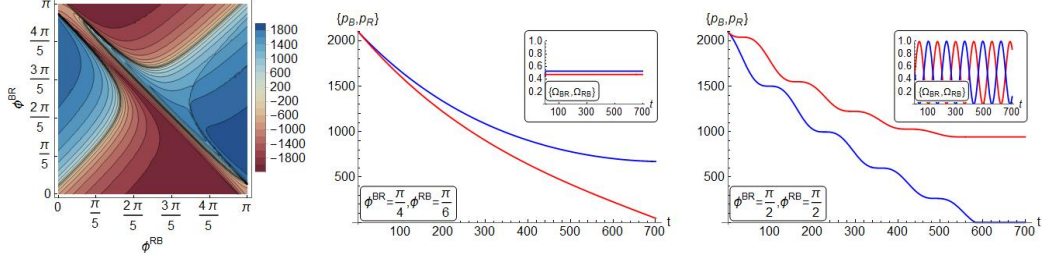


Figure 3.: Left most panel presents contour plot for the value of p_{final} generated from Eqs.(6,10), varying the frustration parameters ϕ^{BR} and ϕ^{RB} . Colours are chosen to match where Blue or Red win the engagement. The middle and right most panels give examples of the the Lanchester trajectories for specific choices of frustration parameters. Additionally, the insets of the middle and right most plots show the dynamics with respect to time of the organisational component of each of Blue and Red’s effectiveness, given in Eq.(9).

The left hand panel of Fig.3 gives the contour plot for p_{final} of value for value of p_{final} generated from Eqs.(6,10), while varying the frustration parameters ϕ^{BR} and ϕ^{RB} . We colour code to highlight where one side or the other wins the engagement. We note although the contour plot does possess some symmetry, Red generally does better than Blue by possessing a wider range of parameter across the space of values that provide for Red victory. This is a consequence of Red’s more connected network structure creating a degree of greater robustness even though the couplings of Blue and Red, respectively, are such as to give the more poorly connected Blue a ‘fighting chance’, reflected in the degree of symmetry seen in the left-most panel of Fig.3. The majority of the asymmetry is focused in the diagonal connecting the points $(0, \pi)$ and $(\pi, 0)$; along this diagonal Red does comparatively better than Blue. By visual inspection we observe that along this diagonal the *cross over* from favourable outcomes for Red to Blue is very sharp, indicated by the bold black lines. These sharp cross overs are in contrast to the gradual contour changes in other regions of the map.

In the middle and right panels we present Lanchester trajectories for two specific choices of frustration parameters. The middle panel’s trajectories, with choice $(\phi^{BR}, \phi^{RB}) = (\pi/4, \pi/6)$, decay approximately exponentially with Blue winning the engagement. The trajectories in the right most panel, for $(\phi^{BR}, \phi^{RB}) = (\pi/2, \pi/2)$, show quasi-periodic decay but with Red victory. The insets in both these panels show the value of the organisational effects over time reflected in the Ω factors that themselves depend on the C2 dynamics. Indeed, the slightly better and flat synchronisation of Blue in the middle panel is consistent with the decay of the Lanchester trajectory. Similarly, the oscillations in the right-most panel are consistent with those in the C2 dynamics in the inset where both sides achieve internal synchronisation, but their global phases periodically oscillate. There is no locking between Blue and Red with one or the other sustaining a lead in decision state. In other words, as Blue and Red agents pass each other in decision state they momentarily gain an attritional advantage

seen in the oscillations in p_B, p_R . The fact that Red nonetheless wins that engagement needs deeper explanation, to which we turn now.

2.5. Clustering assumption and simplification

Given that the model detailed in Eqs.(6,10) is a coupled system of nonlinear ordinary differential equations, generally it may only be solved numerically. Nevertheless, as the form of the Kuramoto model is currently unaffected by the Lanchester trajectories, we may leverage the work done on understanding the stability and synchronisation properties of two-network adversarial models with frustrations (Kalloniatis & Zuparic, 2016). Beginning with the assumption that the Blue and Red networks are approximately phase synchronised via

$$\theta_i^B \approx b_i + \Theta_B, \quad \theta_j^R \approx r_j + \Theta_R, \quad \{i, j\} \in \{\mathcal{B}, \mathcal{R}\}, \quad (14)$$

where the quantities b_i and r_j are fluctuations with second order terms (and above) approximately equal to zero, *i.e.* $b_i b_j \approx b_i r_j \approx r_i r_j \approx 0 \quad \forall i, j$. If these perturbations are sufficiently small, then $O_B \approx O_R \approx 1$, and we have the following closed form expression for Δ_{BR} (Kalloniatis & Zuparic, 2016),

$$\Delta_{BR}(t) = 2 \arctan \left[\frac{C - \sqrt{\mathcal{K}} \tanh \left(\frac{t + \text{const}}{2} \sqrt{\mathcal{K}} \right)}{\bar{\omega}_B - \bar{\omega}_R - S} \right] \quad (15)$$

where we have defined,

$$\begin{aligned} \mathcal{K} &\equiv \mathcal{K}(\phi^{BR}, \phi^{RB}) = C^2 + S^2 - (\bar{\omega}_B - \bar{\omega}_R)^2, \\ C &\equiv C(\phi^{BR}, \phi^{RB}) = \frac{d_T^{BR} \zeta_{BR} \cos \phi^{BR}}{|\mathcal{B}|} + \frac{d_T^{RB} \zeta_{RB} \cos \phi^{RB}}{|\mathcal{R}|}, \\ S &\equiv S(\phi^{BR}, \phi^{RB}) = \frac{d_T^{BR} \zeta_{BR} \sin \phi^{BR}}{|\mathcal{B}|} - \frac{d_T^{RB} \zeta_{RB} \sin \phi^{RB}}{|\mathcal{R}|}, \end{aligned} \quad (16)$$

and,

$$d_T^{BR} = \sum_{i \in \mathcal{B}} \sum_{j \in \mathcal{R}} \mathcal{A}_{ij}^{BR}, \quad d_T^{RB} = \sum_{i \in \mathcal{R}} \sum_{j \in \mathcal{B}} \mathcal{A}_{ij}^{RB}, \quad (17)$$

give the number of edges between Blue to Red, and Red to Blue, respectively. In the use-case of the tree versus the random graph $d_T^{BR} = d_T^{RB} = 16$. Here, $\text{const} \in \mathbb{R}$ is set by the initial condition of Δ_{BR} at $t = 0$.

If $\mathcal{K} \geq 0$ in Eq.(15), *i.e.* the cross couplings are sufficiently large to overcome the natural frequency difference, then Δ_{BR} approaches the stable asymptotic limit,

$$\Delta_{BR}^\infty = 2 \arctan \left(\frac{C - \sqrt{\mathcal{K}}}{\bar{\omega}_B - \bar{\omega}_R - S} \right). \quad (18)$$

Contrastingly, if $\mathcal{K} < 0$ then Δ_{BR} remains time-dependent with periodic behaviour.

The transient behaviour of Δ_{BR} for $\mathcal{K} \geq 0$ is also important for combat outcomes since, if a force can initially accelerate ahead to an early advantage even if it is unable to maintain that advantage in the asymptotic state, it may inflict enough damage to ensure victory. We use the derivative of Eq.(15) at $t = 0$ to inspect which force accelerates ahead,

$$\begin{aligned} \dot{\Delta}_{BR}(t=0) &= \frac{-\mathcal{K}}{1 + \left[\frac{C - \sqrt{\mathcal{K}} \tanh\left(\frac{const\sqrt{\mathcal{K}}}{2}\right)}{\bar{\omega}_B - \bar{\omega}_R - S} \right]^2} \left[\frac{\text{sech}^2\left(\frac{const\sqrt{\mathcal{K}}}{2}\right)}{\bar{\omega}_B - \bar{\omega}_R - S} \right] \\ &= \bar{\omega}_B - \bar{\omega}_R + S, \end{aligned} \quad (19)$$

where the second line in Eq.(19) follows from applying the initial condition $\Delta_{BR}(t=0) = 0$, leading to $const = \frac{2}{\sqrt{\mathcal{K}}} \text{arctanh}\left(\frac{C}{\sqrt{\mathcal{K}}}\right)$. Thus, from Eq.(16) for S , Eq.(19) reveals that forces with faster mean natural frequencies or have higher cross-coupling coefficients (with the appropriate frustration) are able to gain an initial phase advantage over their adversaries leading to an early increase in their organisational combat component. Specifically, for $\phi^{BR} = \phi^{RB} = \frac{\pi}{2}$, as in the right-most panel of Fig.3, $S = 0$ so that $\dot{\Delta}_{BR}(t=0) = -0.048 < 0$ giving Red a slight transient advantage.

Using the same set-up as numerically studied previously, we plot p_{final} generated from the Lanchester trajectories in Eq.(10) using the assumption that $O_B \approx O_R \approx 1$, and applying the analytic time dependent (Eq.(15)) and asymptotic (Eq.(18)) form of Δ_{BR} in Figure 4. The left most panel in Fig.4 gives the contour plot of p_{final} generated from Eqs.(10,15), *reducing from 44 to 2 the dimension of the underlying system of differential equations*. Comparing with the contour plot given in Figure 3, we see that the clustering assumption fares well in this parameter regime.

The right most panel of Fig.4 shows the equivalent contour plot for p_{final} , but with the time dependent expression for Δ in Eq.(15) replaced with the asymptotic expression Δ^∞ , given by Eq.(18), which is only valid in the region $\mathcal{K} \geq 0$. We can notice that the *bump* present in the left hand panel, yet absent in the right hand panel, is the effect of the transient system behaviour before the system attains steady-state. That is, if Blue locks ahead asymptotically *and* accelerates ahead during the transient dynamics, it is able to obtain additional benefit. This then explains why in the right-most case in Fig.3 Red is able to win - due to its initial transient trajectory.

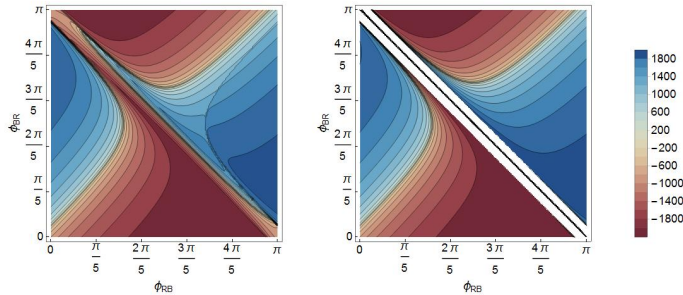


Figure 4.: Left most panel presents contour plot of p_{final} generated from Eqs.(10,15). The right most panel shows the equivalent contour plot for p_{final} , with the asymptotic expression Δ^∞ which is only valid in the region $\mathcal{K} \geq 0$, given by Eq.(18).

2.6. Introducing feedback into the organisational dynamics

We now provide the most obvious generalisation of this model, where Lanchester combat outcomes feed back into the Kuramoto decision making dynamics. A straightforward way to achieve this is to attenuate the various cross couplings with a function of the current and initial populations:

$$\begin{aligned} \sigma_B &\mapsto f(p_B(t), p_{B0}) \cdot \sigma_B, & \sigma_R &\mapsto f(p_R(t), p_{R0}) \cdot \sigma_R, \\ \zeta_{BR} &\mapsto g(p_B(t), p_{B0}, p_R(t), p_{R0}) \cdot \zeta_{BR}, & \zeta_{RB} &\mapsto g(p_R(t), p_{R0}, p_B(t), p_{B0}) \cdot \zeta_{RB}. \end{aligned} \quad (20)$$

In other words, as a force suffers attrition its ability to couple changes. Depending on context, when a particular force loses resource/population agents may lose focus on staying ahead of the adversary's organisational decision cycles, in which case $g(p, p_0) = \frac{p}{p_0}$; or expend more effort on staying ahead of the adversary's decision cycles, in which case $g(p, p_0) = \frac{1}{p/p_0 + \epsilon}$ for small $\epsilon > 0$. Situations for different g are visualised in Figs.5 and 6. We also explored different values of f , only to produce contours very similar to Fig.3. We explore the reason for this in the following.

In Fig.5, we present results for the particular choice

$$f_B = f_R = 1, \quad g_B = \frac{p_B}{p_{B0}}, \quad g_R = \frac{p_R}{p_{R0}}, \quad (21)$$

which represents the scenario where suffering attrition results in the degradation of the ability to stay ahead of the adversary's collective decision cycle. Focusing on the contour plot on the left hand panel, we see that the effect of the attenuation given in Eq.(21) greatly expands the Red force's ability to win engagements compared to where attrition makes no impact on C2. Importantly, there are now whole regions — approximately $\phi^{RB} \in (3\pi/10, \pi/2)$ — where Red wins the engagement *regardless* of the choice Blue makes with its frustration parameter. This is a new situation which does not appear in the equivalent contour in Figure 3, and highlights the difference in network topology, and the importance of a force maintaining focus on the adversary's decision cycles.

The middle panel, with the choice $(\phi^{BR}, \phi^{RB}) = (\pi/4, \pi/6)$, presents a Lanchester trajectory where Blue is (barely) ahead for the majority of the engagement, but is overtaken at approximately $t = 700$ and proceeds to extinction shortly after. The inset helps to understand how this marked change occurs noting the two-way influence between C2 and combat dynamics. As attrition sets in for both forces, and therefore degradation of coupling through Eq. (21), neither is able to build up significant coherence with Ω values remaining around 0.5. Nevertheless, early in the competition ($t \approx 300$) Red gains an albeit narrow advantage through a relatively superior coherence across its members' decision states (inset). This is a consequence of its superior more connected network structure – again, providing robustness. This in turn translates into a deceleration in its attritional losses. Even though both forces reach a point of parity at $t = 700$, the superior decision coherence of Red at this stage means it ceases to take losses while Blue's trajectory is unchanged. As Blue suffers further attrition its capacity to maintain decision coherence collapses. Red's coherence only continues to improve because it is able to stabilise it's locking ahead of Blue (the attenuation is in g) and therefore there ceases to be a conflict between that and its internal drive for synchronisation.

Contrasting this with the right panel of Fig. 5, for $(\phi^{BR}, \phi^{RB}) = (\pi/2, \pi/2)$, we see

the Red force staying ahead for the entirety of the engagement. In the insets of both of these panels which show the value of the organisational factors Ω over time, we notably witness much more non-monotonicity than the equivalent insets in Fig.3.

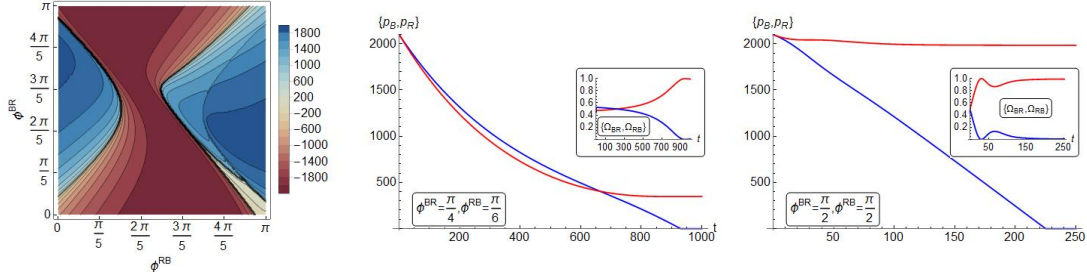


Figure 5.: Left most panel presents contour plot for the value of p_{final} generated from Eqs.(6,10), using the attenuation given in Eq.(21). The middle and right-most panels give examples of the the Lanchester trajectories for specific choices of frustration parameters. Additionally, the insets of the middle and right-most plots show the dynamics with respect to time of the organisational component of each of Blue and Red’s effectiveness, given in Eq.(9).

Contrastingly, in Fig.6, we present results for the attenuation choice

$$f_B = f_R = 1, \quad g_B = \frac{1}{\frac{p_B}{p_{B0}} + 10^{-3}}, \quad g_R = \frac{1}{\frac{p_R}{p_{R0}} + 10^{-3}}, \quad (22)$$

which emulates the opposite scenario, where suffering losses results in increased effort to stay ahead of the adversary’s collective decision cycle. Visual inspection of the contour plot on the left hand panel of Fig.6 shows that the attenuation given in Eq.(22) largely puts both forces on an even playing field; blue and red regions of the plot are nearly equal in area. Interestingly, we see that large regions of the (ϕ^{BR}, ϕ^{RB}) parameter space now result in stalemate scenarios for the Blue and Red forces, especially in the middle and along the diagonals. This situation is absent from Fig.3. From the contour in Figure 6, we see that the attenuation in Eq.(22) almost eliminates the effects of intrinsic differences between Blue and Red (native frequencies and/or network structure).

The middle panel, with choice $(\phi^{BR}, \phi^{RB}) = (\pi/4, \pi/6)$, presents a fairly uninteresting Lanchester trajectory, which typifies the behaviour witnessed in the blue and red coloured regions of the contour plot with a clear winner. In real contrast to this, the right panel, for $(\phi^{BR}, \phi^{RB}) = (\pi/2, \pi/2)$, exemplifies the extent of the impact the attenuation of Eq.(22) when one force gains an advantage over the other. Notably, for small times, as the difference between Red and Blue gets too large, the organisational effects (see inset) oscillate rapidly, causing the populations to achieve parity. As time evolves the behaviour repeats quasi-periodically, until Red diminishes linearly at $t \approx 700$.

In an effort to explain this sudden drop in Red’s effectiveness and lack of quasi-periodicity in the Lanchester trajectories past $t = 700$ in the right-most panel of Fig.6, we plot the corresponding time dependence of the order parameters, O_B and O_R from Eq.(4), for these two specific instances in Figure 7. The left hand plot, for $(\phi^{BR}, \phi^{RB}) = (\pi/4, \pi/6)$, displays highly synchronised Blue and Red order parameters, meaning that the multiplicative O -terms contained within Eq.(9) are approximately

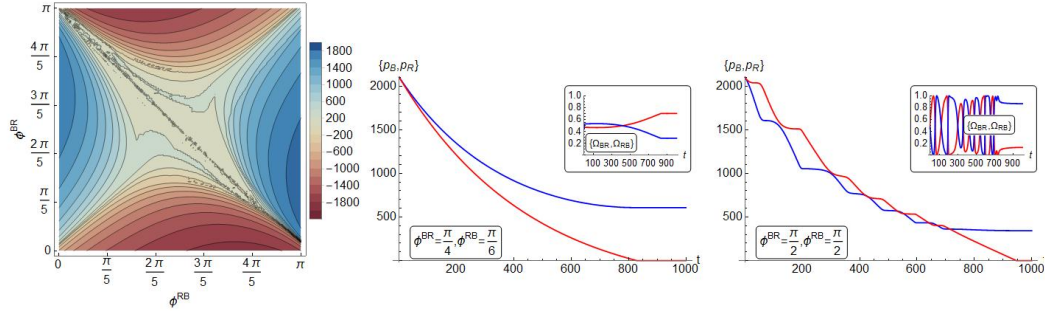


Figure 6.: Left most panel presents contour plot for the value of p_{final} generated from Eqs.(6,10), using the attenuation given in Eq.(22). The middle and right most panels give examples of the the Lanchester trajectories for specific choices of frustration parameters. Additionally, the insets of the middle and right-most plots show the dynamics with respect to time of the organisational component of each of Blue and Red’s effectiveness, given in Eq.(9).

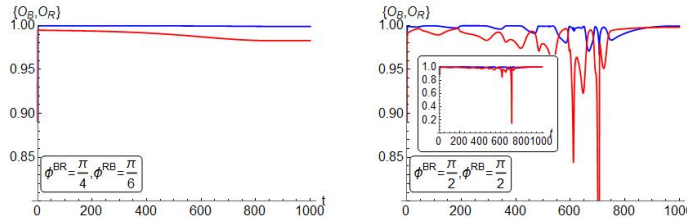


Figure 7.: Plots of the time dependent order parameters — Eq.(4) — corresponding to the Lanchester trajectories displayed in Figure 6. The inset on the right hand plot has the same parameter values as the parent panel and displays a larger range to offer more perspective.

equal to unity, and do not negatively influence the organisational contribution to the force effectiveness. The right hand plot however shows a markedly different scenario, with both trajectories highly variable, and although the Blue order parameter stays close to unity for all t , the Red order parameter deviates significantly at multiple times, with the largest occurring at approximately $t = 700$. This significant deviation causes the multiplicative O_R -term for Red’s internal organisational effectiveness to plummet to zero. Moreover, we also see that Red’s organisational combat factor Ω in the inset of the right plot of Fig.6 subsequently loses its ability to rise in a quasi-periodic manner. In summary, because the Red force excessively tightens in relation to Blue after suffering attrition its internal decision-making coherence has degraded, which in turn impacts on its combat effectiveness. Can such second-order effects be computed semi-analytically?

2.7. *Semi-analytic approach in presence of combat feedback on organisational dynamics*

We perform a dimensional reduction approximation to the system of Eqs.(6,10), in a manner equivalent to (Kalloniatis & Zuparic, 2016) in order to exploit the approxima-

tion given by Eq.(15). Because Lanchester terms appear now in the phase dynamics, the previous approach is insufficient. This is a rather lengthy calculation relegated to the Appendix. The derivation exploits properties of the graph Laplacian spectra for the Blue and Red force networks (Bollobás, 2013,P). Critically, to simplify we assume that each force is close to internal synchronisation of its decision cycles, $O_B, O_R \approx 1$. These considerations give:

$$\begin{aligned} \dot{\Delta}_{BR} &= \bar{\omega}_B - \bar{\omega}_R - \left[\frac{\zeta_{BR}}{|\mathcal{B}|} g(p_B) \sin(\Delta_{BR} - \phi_{BR}) d_T^{BR} + \frac{\zeta_{RB}}{|\mathcal{R}|} g(p_R) \sin(\Delta_{BR} + \phi_{RB}) d_T^{RB} \right], \\ \dot{p}_B &= -\kappa_{RB} \frac{1 - \sin(\Delta_{BR})}{2} p_R \mathcal{H}(p_B), \quad \dot{p}_R = -\kappa_{BR} \frac{1 + \sin(\Delta_{BR})}{2} p_B \mathcal{H}(p_R). \end{aligned} \quad (23)$$

In the Appendix we detail why Eq.(23) is independent of the feedback terms f , consistent with our observations that choices for these functions played minimal role in the contour plots. We note that if the remaining feedback term g equals unity, then the differential equation for Δ_{BR} in Eq.(23) is solvable, leading to the expression already given in Eq.(15). We give contour plots of the outputs of Eq.(23) in Fig.8, which should be compared with those in Figs.5 and 6.

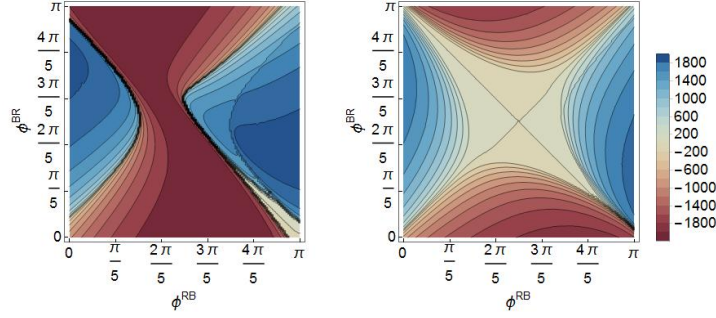


Figure 8.: Contour plots of the dimensionally reduced system given in Eq.(23) with the same parameter inputs chosen to produce Figures 5 and 6. The left plot presents the case $g(p) = p/p_0$, which can be directly compared to the contour plot in Figure 5. Additionally, the right panel applies $g(p) = (p/p_0 + 10^{-3})^{-1}$, and hence can be directly compared to the contour plot of Figure 6.

From visual inspection, we see that the choice $g(p) = p/p_0$ in the left panel serves to accentuate Red’s ability to win engagements, with the attenuation term lessening each force’s ability to pursue their intent of staying ahead of their adversary’s global phase as they suffer attrition. Contrast to this to the right most-plot in Fig. 8, we see that the choice $g(p) = (p/p_0 + 10^{-3})^{-1}$ largely levels the ability for Red and Blue to win engagements. However, as found in Fig. 7, the tightening of a force’s attention on the adversary that this models can become out of balance for the requirement of internal coherence, as witnessed in Sec. 4.4 of (Kalloniatis & Zuparic, 2016) — explaining the difference in detail between the right panel in Fig.8, and the equivalent contour plot in Fig.6. Notably, in Fig.8 we are not witnessing any internal network decoherence of the force as the approximations used in the Appendix for Eq.(23) exclude this behaviour.

To summarise this section: using a representation of homogeneous forces, though networked in their decision-making, we have established the principles for unifying the Lanchester and Kuramoto models. We did this for both cases where attrition does not, or does, impact on the ability of the forces to conduct C2. Additionally, we see

that, with some considered approximations, we are able to reproduce, and analytically understand, many of the predictions of the models for the outcome of battle. We now take these principles and insights to highly non-homogeneous forces.

3. Embedding Lanchester into a network: the networked Lanchester-Kuramoto-Sakaguchi model

We finally present the model we have been building up to, a representation for two distributed inhomogeneous forces in combat, where their internal decision-making dynamics is in tension with their seeking to achieve tactical decision-making ahead of the adversary. To the degree that they have decision advantage they gain a combat advantage. Moreover, they have the capacity to shift force elements dynamically through a network adapting to the dynamics of battle, where we build in the Lanchester-manoeuvre parts of (Kalloniatis *et al.*, 2020a).

3.1. Model definition

To generalise the model given in Sec.2 by placing the Lanchester component on a network, introducing manoeuvre, we propose the following $2|\mathcal{K}|$ -dimensional system,

$$\dot{\theta}_i = \mathcal{H}(p_i) \left[\omega_i - \sum_{j \in \mathcal{K}} \mathcal{H}(p_j) \mathcal{K}_{ij} \sigma_{ij} \sin(\theta_i - \theta_j - \Phi_{ij}) \right], \quad i \in \mathcal{K}, \quad (24)$$

$$\begin{aligned} \dot{p}_i = \mathcal{H}(p_i) \left[\sum_{h \in \mathcal{M}} \mathcal{H}(p_h) \mathcal{M}_{ih} \frac{\Gamma_{i,h} + \Gamma_{h,i}}{2} (\delta_h p_h - \delta_i p_i) \frac{\cos(\theta_h - \theta_i) + 1}{2} \right. \\ \left. - \sum_{k \in \mathcal{E}} \mathcal{H}(p_k) \mathcal{E}_{ik} \kappa_{ik} p_k d_k \frac{\sin(\theta_k - \theta_i) + 1}{2} O_k \right], \quad i \in \mathcal{K}. \end{aligned} \quad (25)$$

The organisational component Eq.(24), is largely unchanged from Eqs.(2,3) apart from additional Heaviside factors that ensure force elements reaching zero (or some other threshold) are incapable of further participating in the dynamics. The need for this arises here specifically because of the localised interaction between decision states (Kuramoto phases) θ_i and individualised combat element force strengths p_i . Quite simply, if an individual force element is extinguished it ceases to couple to partners – the *internal* factor $\mathcal{H}(p_i)$ in Eq. (24) – and it ceases to cycle through its own disconnected decisions – the *external* factor $\mathcal{H}(p_i)$ in Eq. (24).

Focusing on the networked Lanchester terms Eq.(25), we distinguish between *manoeuvre* \mathcal{M} and *engagement* \mathcal{E} components of the network \mathcal{K} :

$$\mathcal{K} = \underbrace{\begin{bmatrix} 0 & \mathcal{A}^{BR} \\ \mathcal{A}^{RB} & 0 \end{bmatrix}}_{\equiv \mathcal{E}} + \underbrace{\begin{bmatrix} \mathcal{B} & 0 \\ 0 & \mathcal{R} \end{bmatrix}}_{\equiv \mathcal{M}}. \quad (26)$$

Additionally, we define the *local order parameter* O_k , at each node k , via

$$O_k = \frac{\left| \sum_{m \in \mathcal{M}} \mathcal{M}_{km} \mathcal{H}(p_m) e^{\sqrt{-1}\theta_m} \right| + \epsilon_2}{\sum_{m \in \mathcal{M}} \mathcal{M}_{km} \mathcal{H}(p_m) + \epsilon_2}, \quad (27)$$

which measures how synchronised each oscillator is with its nearest neighbour. In contrast to O_B, O_R used previously, the normalisation here is time-dependent, and may vanish, hence the regularisation ϵ_2 . It should be clear how this insertion of O_k in the last term of Eq.(25) with the sine factor, generalises the principles in Eq.(10).

The parameters δ and d in Eq.(25) are defined by,

$$\delta_k = \frac{1}{\sum_{m \in \mathcal{E}} \mathcal{E}_{km} p_m + 1}, \quad d_k = \frac{1}{\sum_{m \in \mathcal{E}} \mathcal{E}_{km} \mathcal{H}(p_m) + \epsilon_2}, \quad (28)$$

introduced in (Kalloniatis *et al.*, 2020a), with δ moderating the flow of resource in the internal networks, and d moderating the effectiveness of the engagement. We reiterate that ϵ_2 is a small real number, chosen in this work specifically by $\epsilon_2 = 10^{-20}$.

Eq.(25) draws upon the model developed (without C2) in (Kalloniatis *et al.*, 2020a). The differences of this extension are characterised by distributing resource across network nodes rather than a global total; dividing the combat effectiveness of a node by the number of concurrent engagement connections d_k ; replacing the network-average phase difference term Δ_{BR} , with a nodal nearest neighbour adversary factor, $\theta_k - \theta_i$; and replacing the global order parameter O_B and O_R by a local per-node check against any other nodes connected along the manoeuvre network, O_k , defined in Eq.(27).

The manoeuvre mechanism given in the first line of Eq.(25) allows node h with non-zero resource and manoeuvre connection to node i ($\mathcal{M}_{ih} = 1$) to share resource according to the average of their manoeuvre constants ($\frac{\Gamma_{ih} + \Gamma_{hi}}{2}$), multiplied by the difference in force ratios between the sharing nodes and the total adversarial population among their respective engagements ($\delta_h p_h - \delta_i p_i$), and the extent to which their decision making is in agreement ($\frac{\cos(\theta_h - \theta_i) + 1}{2}$). Alternately, \mathcal{M} may be thought of as a network regulating the force-flow of through the combat engagement.

The choice of the term ‘1’ in the denominator of δ in Eq.(28) represents a ‘standing force’ that a non-combat node wishes to maintain. If replaced by a number less than unity, non-combat nodes give up their resource rapidly to engaged nodes; if greater than unity, all nodes distribute resource evenly with little regard for engagements.

The matrix terms κ and Γ control the rates of physical effectiveness and manoeuvre, respectively:

$$\kappa = \begin{bmatrix} 0 & \kappa_{BR} \\ \kappa_{RB} & 0 \end{bmatrix}, \quad \Gamma = \begin{bmatrix} \gamma_B & 0 \\ 0 & \gamma_R \end{bmatrix}. \quad (29)$$

It is important to note that the choice of manoeuvre using the difference in force ratios is a heuristic. Indeed, many historical engagements have been decided by the ability to rapidly concentrate and distribute forces as required. In (Kalloniatis *et al.*, 2020a), it was seen that optimised networks (without an explicit dynamical representation of C2) with such a heuristic delivered structures that resembled Manoeuvre Theory concepts, such as Feints and Disruptive Fire.

The current choice for δ in this work disperses resources among engagements to match the opposition, rather than exploiting weaknesses with targeted force concen-

trations due to application of human initiative. Nevertheless, one can argue that forces behave in a somewhat diffusive way in various contexts. Although manoeuvres resulting in localised concentrations often require knowledge of the state of combat beyond the nearest neighbour, if agents can only act on local information *in lieu* of a network-wide strategy, this may be the most optimal choice available. Moreover, particularly risk-averse decision-makers may still order this as a global strategy despite being sub-optimal in many scenarios as seen by the French Military “penny packet” distribution of superior armour in the prelude to the WWII Battle for France. At any rate, we save the more advanced heuristics, such as adversarial dynamic reallocation of forces, to future studies.

A final difference between the global (Eqs.(2,10)) and networked (Eqs.(24,25)) Lanchester models is that when nodes are extinguished we set the corresponding *phase velocity* to zero; ‘death’ of the combat element freezes its decision-making capability. While not strictly necessary, as empty nodes cannot affect their nearest neighbours, it does have the advantage of reducing the dimensionality of the dynamical system as time progresses which slightly improves computation time.

3.2. *Pairwise Lanchester feedback and numerical comparison*

Similar to Sec.2.6, we now propose the following attenuation functions for the feedback of Lanchester dynamics into the Kuramoto-Sakaguchi component of the model in Eq.(24)

$$\begin{aligned} \sigma_B &\mapsto \frac{2p_j^B}{p_i^B + p_j^B} \cdot \sigma_B, & \sigma_R &\mapsto \frac{2p_j^R}{p_i^R + p_j^R} \cdot \sigma_R, \\ \zeta_{BR} &\mapsto \frac{2p_i^B}{p_i^B + p_j^R} \cdot \zeta_{BR}, & \zeta_{RB} &\mapsto \frac{2p_i^R}{p_i^R + p_j^B} \cdot \zeta_{RB} \end{aligned} \quad (30)$$

The attenuations multiplying the intra-network couplings σ here mean that nodes with higher resource have more weight over their nearest neighbours’ (in the manoeuvre network) decision making, and are able to track an engaged adversary better if those respective neighbours and adversaries have less resource. The factor of ‘2’ in the numerator ensures that when resources are equal, the resource coefficient is unity. Also, the attenuations multiplying the couplings ζ , as with the equivalent in Eq.(21), sharpen the transitions which reinforce early winning trajectories. Before detailing the use-cases of the networked model defined in Sections 3.1–3.2, Table 2 presents the parameter values applied for each of the use-cases.

Table 2.: Summary of parameter values used for the three use-cases in Sections 3.3–3.5.

parameters	use-case 1	use-case 2	use-case 3
$\{\sigma_B, \sigma_R\}$	$\{8, 0.5\}$	$[0, 5]$	$\{[0, 0.5], 0\}$
$\{\bar{\omega}_B, \bar{\omega}_R\}$	$\{0.503, 0.551\}$	1 and 1.009	$\{1.104, 0\}$
$\{\zeta_{BR}, \zeta_{RB}\}$	0.4	$\{0, 0.1, 0.5, 1, 1.5, 2\}$ and $\{0, 1.25, 3\}$	0.5
$\{\kappa_{BR}, \kappa_{RB}\}$	0.005	0.1	$\{[0, 0.03], 0.01\}$
$\{\phi^{BR}, \phi^{RB}\}$	$[0, \pi]$	$\frac{\pi}{4}$	$\{\frac{\pi}{4}, 0\}$
$\{\gamma_B, \gamma_R\}$	1	1	$\{1, 5, 10, 15\}, 0\}$

3.3. Numerical calculations with use-case 1

Due to its complexity, this model must be solved numerically. However, to enable potential understanding of underlying mechanisms for model behaviour, we additionally look at the model through the lens of the semi-analytic approximation, detailed in Section 2.7, when appropriate. To facilitate the embedding of manoeuvre here, the \mathcal{E} and \mathcal{M} adjacency matrices in Eq.(26) were respectively introduced to define engagement and manoeuvre network connections. Although these are fundamentally different, we simplify by identifying Kuramoto intra-network connection with manoeuvre connections, and Kuramoto inter-network connection with engagement/combat connections. We thus initially explore the same use-case for the global model.

In Fig.9 we give plots of Eq.(25), which should be compared to the contours in Figs.3 and 5 for the global model. We run the networked model on the same scenario and parameter values as described in Sec.2 to provide comparison. With the generalised model the additional parameters are set as follows: the new manoeuvre constant is set to $\Gamma = 1$ between all manoeuvre connections; the total population of 21 nodes for each network is evenly distributed 100 resources per node for both Blue and Red. Lastly, we generalise the expression of p_{final} via,

$$p_{final} = \sum_{i \in \mathcal{B}} p_i^B(t)|_{t=t_{final}} - \sum_{i \in \mathcal{R}} p_i^R(t)|_{t=t_{final}}. \quad (31)$$

from Eq.(13) to account for the fact the resource is now distributed through each network.

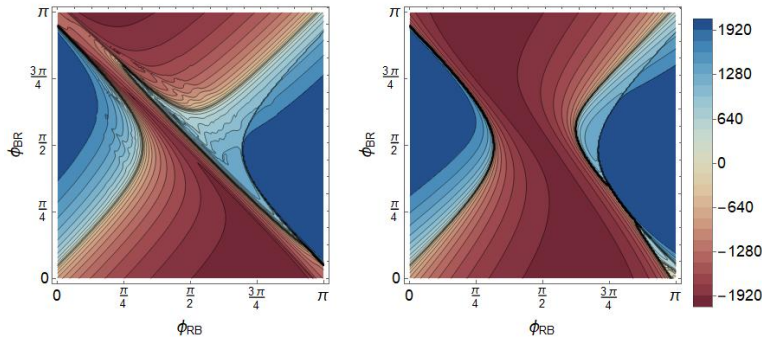


Figure 9.: Contour plots of combat outcomes against frustrations $\phi_{RB}, \phi_{BR} \in \mathbb{S}^1$ for use-case 1. Left and right panels give Network Lanchester (Eq.(25)) outcomes without and with cross-coupling feedback of the form in Eq.(30), respectively.

Overall, visual inspection reveals that both panels in Fig.9 which display the outputs of the networked Lanchester model are very similar to their global counterparts in Figs.3 and 5. For scenarios which exhibit a relatively high degree of intra-network synchronisation, as well as a homogeneous distribution of resource and engagement, the networked Lanchester model in Eq.(25) essentially reduces to the global formulation given in Eq.(10). This is to be expected given that homogeneity removes the necessity to manoeuvre resource as all force ratios are equal from the start of combat. Attrition dominates. This result justifies the application of the global Lanchester analysis, using Eq.(10), to understand behaviours seen in the networked Lanchester expressions of Eq.(25), when in the appropriate regimes. However, as we are interested in exactly

those scenarios where attrition doesn't dominate over manoeuvre, we now consider a stylised inhomogeneous case.

3.4. Use-case 2: The ‘Fighting Fish’

To highlight the nuances of the networked model, we consider a heterogeneous scenario where the trade-off between manoeuvre and engagement effectiveness has no analogue in the global Lanchester model. We construct a network and population distribution in which the ability to manoeuvre is implicitly rewarded. Both the Blue and Red networks, \mathcal{B} and \mathcal{R} , consist of a ring with a hub node that is connected to two additional nodes as depicted in Figure 10. Combat occurs in one-to-one engagements across the first three nodes, *i.e.* the engagement adjacency matrix \mathcal{E} consists of Blue node j connected to Red node j , for $j \in \{1, 2, 3\}$. Viewing these two graphs with mutually combat nodes adjacent to each other suggests the name ‘fighting fish’.

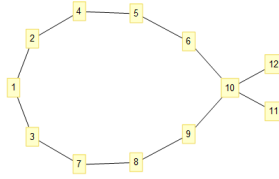


Figure 10.: Graph diagram of the Blue and Red networks, \mathcal{B} and \mathcal{R} .

Initially, resources are distributed unevenly, with $p_1 = p_2 = \dots = p_{10} = 10$, and $p_{11} = p_{12} = 100$, most on the opposite side of the engagement point. The force capable of shifting these reserves to the engagement faster than the opposition fights achieves advantage. We set the frustrations $\phi_{RB} = \phi_{BR} = \frac{\pi}{4}$, the manoeuvre constants $\gamma_B = \gamma_R = 1$, and the lethality constants $\kappa_{RB} = \kappa_{BR} = 0.1$, and vary the intra-network internal couplings σ_B and σ_R , with both inter-network couplings $\zeta_{BR} = \zeta_{RB} = \zeta$. We equate the natural frequencies, $\omega_B = \omega_R = 1$, and equi-space the initial node phases within $[-\frac{\pi}{4}, \frac{\pi}{4}]$; we include the feedback Eq.(30) so capability to rapidly manoeuvre provides a benefit to adversarial decision making. Thus any resulting combat advantage follows from coupling and network structure. We evolve the system to $t_{final} = 10^3$ and plot Eq.(31) for various ζ in Fig.11.

Despite the structural symmetry between the forces we see in Fig.11 a rich picture as inter-network coupling increases, with multiple regions and transitions from competing engagement and organisational effects. Across the panels of Fig.11 we observe the propagation of particular front.

As inter-network coupling ζ_{BR} and ζ_{RB} increases, the phase oscillators attached to engagement nodes synchronise less and less with their respective network's non-combat nodes, while potentially frequency synchronising with their corresponding adversary. Conversely, increasing intra-network coupling σ_B, σ_R has the tendency to enable all nodes within Blue or Red to synchronise collectively. These considerations explain the diagonal symmetry of the plots.

In detail, for $\zeta = 0$, nodes within each network experience no tension from inter-network interaction. Increasing intra-network coupling here gives for each a larger local order parameter and nearest-neighbour agreement, boosting combat effectiveness and speed of resource reallocation. At $\zeta = 0.1$, with inter-network coupling, engagement nodes start to achieve a phase advantage over their respective adversaries. If Red has zero intra-network coupling and Blue slightly increases its own ($\sigma_R = 0, \sigma_B = 0.5$),

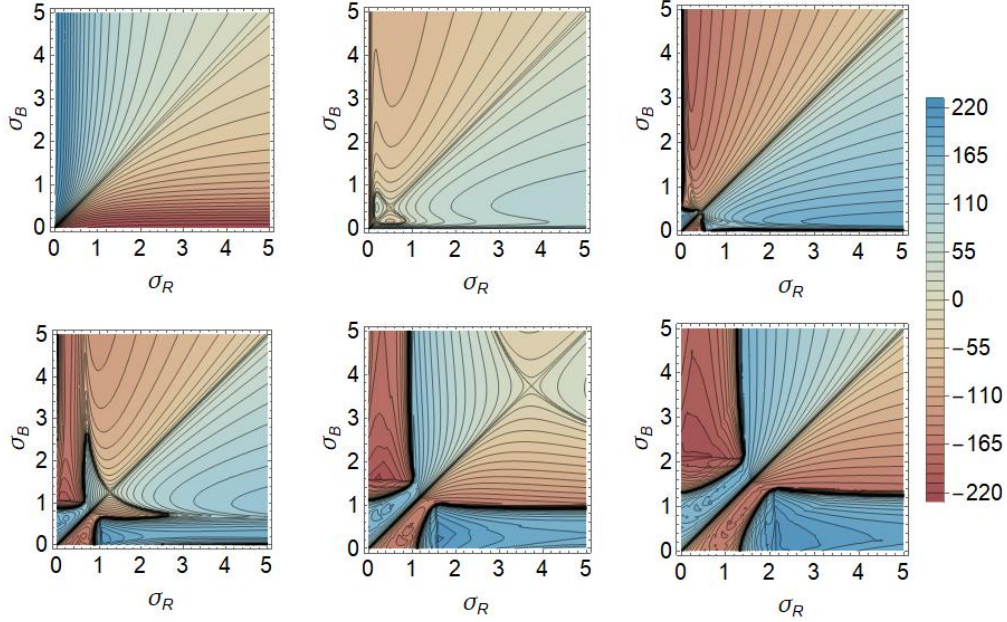


Figure 11.: Engagement outcomes for Eq.(25) with networks \mathcal{B} and \mathcal{R} given use-case 2 in Fig.10. Plots detail the effect of intra-network couplings over the domain $(\sigma_R, \sigma_B) \in [0, 5] \times [0, 5]$, with a simultaneous increase of inter-network couplings $\zeta_{RB} = \zeta_{BR} \equiv \zeta$ from left to right given by $\zeta = \{0, 0.1, 0.5\}$ for the top row, and $\zeta = \{1, 1.5, 2\}$ for the bottom row.

Red engagement nodes achieve a phase advantage over Blue engagement nodes, which are now excessively seeking internal coherence over more rapid manoeuvre. If Red increases intra-network coupling ($\sigma_R = 0.2, \sigma_B = 0.5$), it loses phase advantage from its own excessive effort at internal synchronisation. These effects increase with larger ζ . Overall, the basic reason for the changing structures within a diagonal region is the relative imbalances between decision-speed, resource-manoevre speed, and combat speed resulting in transitions from Blue combat advantage to disadvantage. In Appendix B we examine a path through the landscape to understand more deeply the different variations in these imbalances.

But thus far, with symmetric networks and parameters we have obtained quite regular structures in the landscape. To see a first effect of randomness on this, we sample natural frequencies from a uniform distribution between $[0, 2]$, with a selection of resulting phase plots shown in Fig.12. We see here remnants of the order in Fig.11 but with elements of disorder. The left panel in Fig.12 shows that even for zero inter-network coupling the regions of differentiated behaviour are clearly present as now internal coupling must overcome the tension created by the heterogeneous natural frequency distribution. However, the regions in Fig.12 along diagonals, where there is less likelihood of one force or the other achieving internal synchronisation, display considerable complexity. This suggests that for parameter settings excluding steady-state the outcome is more sensitive to heterogeneous natural frequency distributions. Next we consider a more heterogeneous network structure.

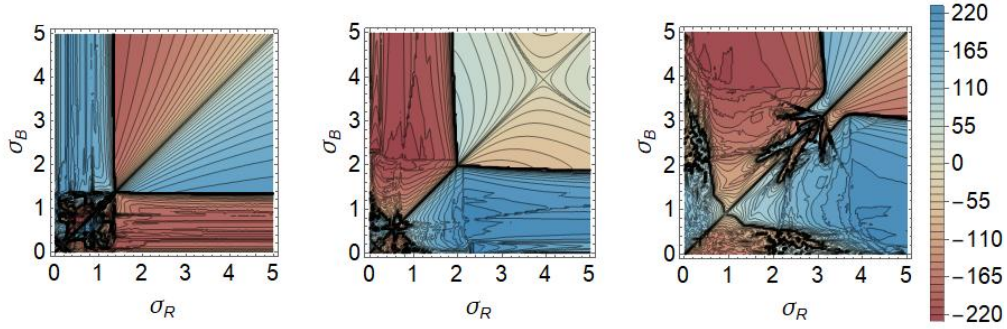


Figure 12.: A selection of phase plots with increasing cross coupling $\zeta = \{0, 1.25, 3\}$ from left to right for use-case 2 with natural frequencies randomly chosen from a uniform distribution over $[0, 2]$.

3.5. Use-case 3: complex network scenario for Blue.

Consider now a Blue force spread across a 50 node network. Here, each of Blue's nodes are resource hubs, with the connections representing routes through which resource may be transported. Contrastingly, the Red force is not networked with 5 detached nodes each of which engage a single Blue node. Thus, linking the equivalently indexed $\{1, \dots, 5\}$ nodes of Blue and Red gives the engagement network \mathcal{E} . We pit Blue's extreme advantage of being networked against a Red overwhelming force concentration. Both Blue and Red possess a total resource 13750. Red evenly divides its force across its detached elements at 2750 per node. Blue has 500 per node of its engagement network, and 250 in each of the remaining nodes. Blue must thus manoeuvre reserves to the first five nodes while ensuring that they are not exhausted immediately by Red's initial superior numerical advantage. Can superior decision making and manoeuvre overcome numerical disadvantage?

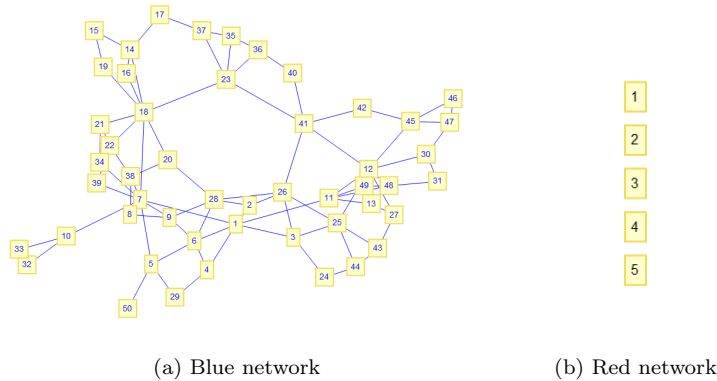


Figure 13.: A graphical depiction of the network structure for each force. Blue is generated from $N_B = 50$ nodes, connected via transportation routes, and the Red network is a series of $N_R = 5$ disconnected nodes. Nodes labelled $\{1, \dots, 5\}$ of each network are connected with their equivalently numbered adversarial counterparts, and hence form the engagement network \mathcal{E} .

Setting $\phi_{BR} = \frac{\pi}{4}$, $\zeta_{BR} = \zeta_{RB} = 0.5$, $\kappa_{RB} = 0.01$, we also set $\phi_{RB} = 0$ to simulate an adversary unaware of the benefits of decision advantage. We choose an instance of

natural frequencies for both Blue and Red from a uniform distribution in the range $[0, 2]$. With the Red force a set of disconnected nodes, we may set $\sigma_R = 0$, $\gamma_R = 0$.

In Fig.14 we compare the global model with manoeuvre rate $\gamma_B = 1$ with the result of sweeping through $\kappa_{BR} \in [0, 0.03]$ and $\sigma_B \in [0, 0.5]$ in the networked model. Visual inspection shows that increasing internal coupling for Blue is significantly more

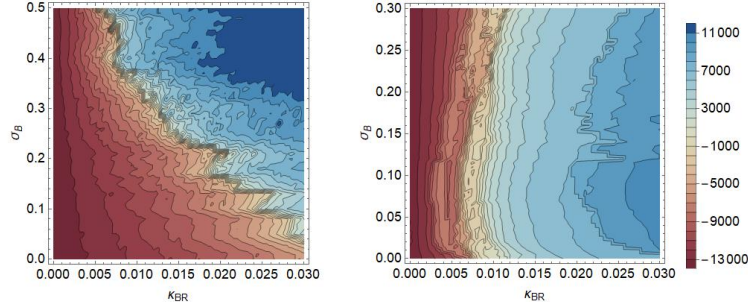


Figure 14.: Comparison of the global Lanchester model of Eq.(10), with the networked counterpart — $\gamma_B = 1$ — for use-case 3.

beneficial in the global than in the networked model. This is due to the global order parameter factor in the former: it penalises systems that are unable to achieve whole of network synchronisation, namely the disconnected Red force, giving Blue a large advantage at high internal couplings. In the networked case, each disconnected Red node automatically has a local order parameter of unity so now Red does not suffer from internal decision incoherence (at low coupling) attenuating its lethality; correspondingly Blue at too low a coupling is not drawing upon the advantages of better connectivity. Compared to the idealised use-case 2, Fig.14 shows no symmetry around a diagonal because the networks are so different. With sufficient internal coupling, Blue is able to overcome Red’s numerical strength by swift decision-making to manoeuvre its resources into the engagement.

Varying the manoeuvre rates to $\gamma_B = \{5, 10, 15\}$, gives Fig.15. The structures seen

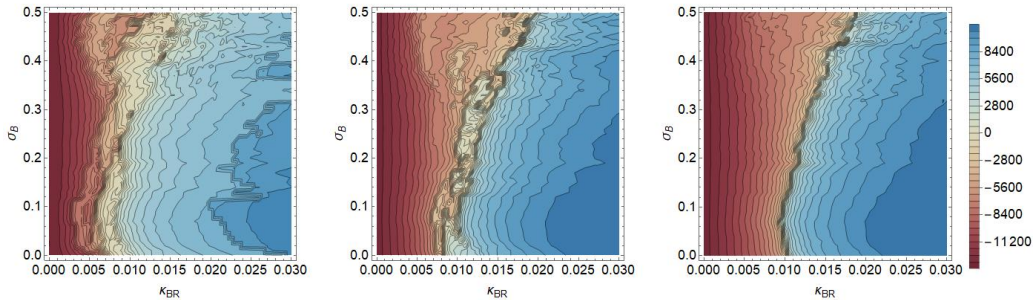


Figure 15.: Plot of networked Lanchester models on use-case 3, with the manoeuvre rate increasing $\gamma_B = \{5, 10, 15\}$ from left to right panels.

in each panel resemble earlier analysis but with more irregularity due to the heterogeneity in use-case 3. As in use-case 2, we see that a degree of intra-network coupling enables the transfer of resource to engagement nodes. *Too much coupling generates diminishing returns*, seen in the blue-red boundary eventually curving away from the vertical axis. High internal coupling reflects an introspective Blue, unresponsive to adversarial decision cycles, with inferior combat power.

Lastly, an increase in the Blue manoeuvre parameter is not strictly advantageous for Blue’s outcome landscape: across the values of γ_B there is no sharp increase of blue regions, only smoothening of the boundary. This suggests a subtle interplay between manoeuvre and network structures (which have not been optimised, unlike in (Kalloniatis *et al.*, 2020a)) that warrants further exploration.

Albeit with a fictitious use-case, Fig.15 allows examination of trade-offs in investment of three types of military systems: weapons, mobile transport, and communications infrastructure which have proxies in the lethality, manoeuvre and internal coupling constants. Against a specific scenario for the adversary and their weapons, and the physical layout of where Blue might intend to confront them we observe a small ‘sweet spot’, where the Blue force trade-offs across these three expenses provide advantage, at slightly lesser lethality than the Red force weapons systems. Naturally, the recommended trade-off point between these investment costs needs also to be tested for sensitivity to variations in choices of natural frequencies (decision-making speeds) and initial conditions, quite straightforward in models of this form. Certainly, a force able to *arbitrarily* increase the lethality of its weapons eventually always wins over an agile manoeuvring opponent: further horizontal shifts to the right by Blue in Fig.15 eventually cross the boundary for victory. This captures the adage, attributed to Stalin, that quantity is its own quality.

4. Conclusion

We have proposed a mathematical model that unifies the warfighting functions of C2 and Manoeuvre with that of Fires — using the celebrated Lanchester equations as substratum. The model draws upon multi-layered networks with different structures available for distributed decision-making, resource manoeuvre, and enemy engagement, thus exploiting aspects of modern complex systems theory. Though deterministic, the model exhibits adaptive dynamics with inhomogeneous forces. For more homogeneous scenarios, semi-analytical approaches may be taken. With inhomogeneity, the model remains parameter-parsimonious, allowing for efficient computational data farming.

The opportunities in future work are considerable. Optimisation of the networks, similar to (Kalloniatis *et al.*, 2020a), should provide insights into ‘tightness’ and centralisation of decision-making to maintain agility of combat forces. Different heuristics for how force elements transfer resources can generate new concepts. Generalising the Lanchester ‘substratum’ from a two- to multi-species Lotka-Volterra system may represent additional actors – non-combatants, non-military agencies – in the operational environment. Adding situation awareness to the present three war-fighting functions through Intelligence, Surveillance and Reconnaissance entities is a next step with a natural spatial embedding of the model in the ‘swarmalator’ formalism (O’Keefe & Bettstetter, 2019), and may still provide a more compact model than (McLemore *et al.*, 2016). Recognising that the ‘enemy gets a vote’ suggests the utility of Game Theory here, analogous to the treatment of the Lanchester model in (Morse *et al.*, 2003), with a first step taken in (Demazy *et al.*, 2018). This paper is thus a significant step in expanding equation based approaches to complex warfare.

Acknowledgements

This work was funded by the Defence Science and Technology (DST) Group of the Department of Defence and conducted under its Modelling Complex Warfighting Strategic Research Initiative.

Appendix A: Calculation of reduced steady-state global Lanchester factor

We begin by substituting the approximation, given by Equation (14), into the defining expression for the Kuramoto-Sakaguchi model (Equation (6)) to obtain

$$\begin{aligned}
 \dot{b}_i + \dot{\Theta}_B &= \omega_i - \sigma_B f(p_B) \sum_{j \in \mathcal{B}} L_{ij}^B b_j - \zeta_{BRG}(p_B) \sin(\Delta_{BR} - \phi_{BR}) d_i^{BR} \\
 &\quad - \zeta_{BRG}(p_B) \cos(\Delta_{BR} - \phi_{BR}) \sum_{j \in \mathcal{B} \cup \mathcal{R}} \mathcal{L}_{ij}^{BR} v_j, \quad i \in \mathcal{B}, \\
 \dot{r}_i + \dot{\Theta}_R &= \nu_i - \sigma_R f(p_R) \sum_{j \in \mathcal{R}} L_{ij}^R r_j + \zeta_{RBG}(p_R) \sin(\Delta_{BR} + \phi_{BR}) d_i^{RB} \\
 &\quad + \zeta_{RBG}(p_R) \cos(\Delta_{BR} + \phi_{BR}) \sum_{j \in \mathcal{B} \cup \mathcal{R}} \mathcal{L}_{ij}^{RB} v_j, \quad i \in \mathcal{R},
 \end{aligned} \tag{32}$$

where d_i^B and d_i^R designate the degree of node i for the Blue and Red network, respectively. Additionally, L^B and L^R are the intra-networks Laplacian matrices of Blue and Red, respectively, given explicitly by,

$$L_{ij}^B = \delta_{ij} d_j^B - \mathcal{B}_{ij}, \quad L_{ij}^R = \delta_{ij} d_j^R - \mathcal{R}_{ij}. \tag{33}$$

Correspondingly, d_i^{BR} signifies the number of edges attached to node $i \in \mathcal{B}$, specifically also connected to nodes from the Red network — and vice versa for d_i^{RB} , *i.e.*

$$d_i^{BR} = \sum_{j \in \mathcal{B} \cup \mathcal{R}} \mathcal{A}_{ij}^{BR}, \quad d_i^{RB} = \sum_{j \in \mathcal{B} \cup \mathcal{R}} \mathcal{A}_{ij}^{RB}. \tag{34}$$

The sum over relevant i 's of each of expression in Equation (34) give d_T^{BR}, d_T^{RB} , introduced in Equation (17). Additionally, the quantities \mathcal{L}^{BR} and \mathcal{L}^{RB} are the inter-network graph Laplacian matrices, given by,

$$\mathcal{L}_{ij}^{BR} = \delta_{ij} d_j^{BR} - \mathcal{A}_{ij}^{BR}, \quad \mathcal{L}_{ij}^{RB} = \delta_{ij} d_j^{RB} - \mathcal{A}_{ij}^{RB}. \tag{35}$$

We note the importance of the graph Laplacian in coupled dynamical systems on networks attributed to the seminal work of (Pecora & Carroll, 1998). The expression v_i in Equation (32) represents the Blue and Red phase fluctuations, via

$$v_i = \begin{cases} b_i, & i \in \mathcal{B} \\ r_i, & i \in \mathcal{R} \end{cases}. \tag{36}$$

We employ the intra-network Laplacians in Equation (32) by exploiting their spanning set of orthonormal eigenvectors, given by

$$\begin{aligned} e_i^{(B,\rho)}, \quad \rho \in \mathcal{B}_E \equiv \{0, 1, \dots, |\mathcal{B}| - 1\}, \quad \sum_{j \in \mathcal{B}} L_{ij}^B e_j^{(B,\rho)} &= \lambda_\rho^B e_i^{(B,\rho)}, \\ e_i^{(R,\rho)}, \quad \rho \in \mathcal{R}_E \equiv \{0, 1, \dots, |\mathcal{R}| - 1\}, \quad \sum_{j \in \mathcal{R}} L_{ij}^R e_j^{(R,\rho)} &= \lambda_\rho^R e_i^{(R,\rho)}. \end{aligned} \quad (37)$$

We have distinguished the indices applied between the network nodes — \mathcal{B} and \mathcal{R} — and the eigen-modes — \mathcal{B}_E and \mathcal{R}_E . Each eigen-mode for Blue and Red is associated with a corresponding positive semi-definite Laplacian eigenvalue, labelled λ^B and λ^R respectively. One can anticipate (Bollobás, 2013) that, as connected graphs, the Blue and Red eigenspaces contain at least one zero-valued Laplacian eigenvalue, labelled specifically as $\lambda_0^B = \lambda_0^R = 0$. The eigenvectors corresponding to these eigenvalues, are conveniently given by the (appropriately normalised) vector consisting of entirely unit-valued entries, *i.e.* $e_i^{(B,0)} = 1/\sqrt{|\mathcal{B}|}$ and $e_j^{(R,0)} = 1/\sqrt{|\mathcal{R}|}$, $\forall i \in \mathcal{B}$ and $j \in \mathcal{R}$.

We further simplify by setting the cross terms — $\sum_{j \in \mathcal{B} \cup \mathcal{R}} \mathcal{L}_{ij}^{BR} v_j$ and $\sum_{j \in \mathcal{B} \cup \mathcal{R}} \mathcal{L}_{ij}^{RB} v_j$ — in Equation (32) to zero. We expand the fluctuations b_i and r_i in the following set of (non-zero) normal eigenmodes

$$b_i = \sum_{\rho \in \mathcal{B}/\{0\}} e_i^{(B,\rho)} x_\rho, \quad r_i = \sum_{\rho \in \mathcal{R}/\{0\}} e_i^{(R,\rho)} y_\rho, \quad (38)$$

into Eq.(32) to obtain

$$\begin{aligned} \sum_{\rho \in \mathcal{B}/\{0\}} e_i^{(B,\rho)} [\dot{x}_\rho + \sigma_B f(p_B) \lambda_\rho^B x_\rho] + \dot{\Theta}_B &= \omega_i - \zeta_{BR} g(p_B) \sin(\Delta_{BR} - \phi_{BR}) d_i^{BR}, \\ \sum_{\rho \in \mathcal{R}/\{0\}} e_i^{(R,\rho)} [\dot{y}_\rho + \sigma_R f(p_R) \lambda_\rho^R y_\rho] + \dot{\Theta}_R &= \nu_i + \zeta_{RB} g(p_R) \sin(\Delta_{BR} + \phi_{RB}) d_i^{RB}. \end{aligned} \quad (39)$$

We now exploit the orthonormality of the Blue and Red Laplacian eigenvectors in Eq.(39) to *solve* for each of the dynamic variables. Beginning with the fluctuations x and y , we apply the appropriate non-zero eigenvectors ($e_i^{(B,\rho_1)}$ for Blue and $e_i^{(R,\rho_2)}$ for Red) to both sides of Eq.(39) and sum both the Blue and Red expressions over all nodes to obtain

$$\begin{aligned} \dot{x}_{\rho_1} &= \sum_{i \in \mathcal{B}} [\omega_i - \zeta_{BR} g(p_B) \sin(\Delta_{BR} - \phi_{BR}) d_i^{BR}] e_i^{(B,\rho_1)} - \sigma_B f(p_B) \lambda_{\rho_1}^B x_{\rho_1}, \quad \rho_1 \in \mathcal{B}_E/0 \\ \dot{y}_{\rho_2} &= \sum_{i \in \mathcal{R}} [\nu_i + \zeta_{RB} g(p_R) \sin(\Delta_{BR} + \phi_{RB}) d_i^{RB}] e_i^{(R,\rho_2)} - \sigma_R f(p_R) \lambda_{\rho_2}^R y_{\rho_2}, \quad \rho_2 \in \mathcal{R}_E/0 \end{aligned} \quad (40)$$

where we have applied the relations,

$$\dot{\Theta}_B = \sqrt{|\mathcal{B}|} \dot{\Theta}_B e_i^{(B,0)}, \quad \dot{\Theta}_R = \sqrt{|\mathcal{R}|} \dot{\Theta}_R e_i^{(R,0)}. \quad (41)$$

Equation (40) gives a convenient linear dynamic expression for each of the fluctuation variables, x and y . We note however that solving for either x or y requires the dynamic

expression for the difference of the global phases, Δ_{BR} , in addition to f and g , coming from the Lanchester dynamics.

Focusing instead on the global phases Θ_B and Θ_R , as opposed to the fluctuations, we apply the appropriate zero eigenmodes ($e_i^{(B,0)}$ for Blue and $e_i^{(R,0)}$ for Red) to both sides of Eq.(39), and sum over the appropriate (Blue or Red) network nodes to obtain

$$\dot{\Theta}_B = \bar{\omega}_B - \frac{\zeta_{BR}}{|\mathcal{B}|} g(p_B) \sin(\Delta_{BR} - \phi_{BR}) d_T^{BR}, \quad \dot{\Theta}_R = \bar{\omega}_R + \frac{\zeta_{RB}}{|\mathcal{R}|} g(p_R) \sin(\Delta_{BR} + \phi_{RB}) d_T^{RB}, \quad (42)$$

where $\bar{\omega}_B, \bar{\omega}_R$ were introduced earlier as the mean of the Blue and Red natural frequencies. Hence, taking the difference of the time derivatives of the two global frequencies in Equation (42) awards us with the defining expression for $\dot{\Delta}_{BR}$. Combining this with the appropriately approximated global Lanchester expressions (Equation 10), *i.e.* $O_B^{global} \approx O_R^{global} \approx 1$, our dimensionally reduced system is given by Equation (23), and restated below for convenience

$$\begin{aligned} \dot{\Delta}_{BR} &= \bar{\omega}_B - \bar{\omega}_R - \left[\frac{\zeta_{BR}}{|\mathcal{B}|} g(p_B) \sin(\Delta_{BR} - \phi_{BR}) d_T^{BR} + \frac{\zeta_{RB}}{|\mathcal{R}|} g(p_R) \sin(\Delta_{BR} + \phi_{RB}) d_T^{RB} \right], \\ \dot{p}_B &= -\kappa_{RB} \frac{1 - \sin(\Delta_{BR})}{2} p_R \mathcal{H}(p_B), \quad \dot{p}_R = -\kappa_{BR} \frac{1 + \sin(\Delta_{BR})}{2} p_B \mathcal{H}(p_R). \end{aligned} \quad (43)$$

Noting that, in contrast to the corresponding time derivative expressions for the fluctuations in Equation (40), the time derivative expression for the difference in global phases given in Equation (23) is independent of the fluctuations x and y , in addition to the Lanchester based feedback term f ; thus in the regimes where $O_B \approx O_R \approx 1$, the presence of f is immaterial, explaining our observation that different f values led to contours similar to figure 3.

Appendix B: Detailed exploration of use-case 2

To explore the different effects in a scenario as simple as use-case 2 detailed in section 3.4, in Fig.16 we set an intermediate inter-network coupling $\zeta_{RB} = \zeta_{BR} = 1.25$ and traverse a particular path through the landscape as follows:

- Point (A) with $(\sigma_R, \sigma_B) = (0, 0)$: Starting at the origin, this is the line of neutral advantage $\sigma_B = \sigma_R$, and thus neither side is able to achieve supremacy. With zero intra-coupling, engagement nodes traverse the decision cycle at a higher frequency than their counterparts due to the frustrations causing a forcing effect.
- Path (A-B): As Blue's internal coupling increases, the engagement and manoeuvre nodes begin to influence each other. Nevertheless, the forcing due to frustration on engagement nodes is still too large for internal coupling to completely overcome, resulting in periodic behaviour of engagement nodes decoupling and re-synchronising with the bulk. Notably, as Blue's internal coupling increases, the engagement nodes spend more time per cycle in the period before decoupling than afterwards.
- Point (B) with $(\sigma_R, \sigma_B) = (0, 0.6)$: In this region Blue obtains an optimal balance between receiving resources fast enough to achieve a numerical advantage and not allowing Red to attain an overwhelming decision (phase) advantage.
- Path (B-C): Further increases to Blue's internal coupling continue to afford Red

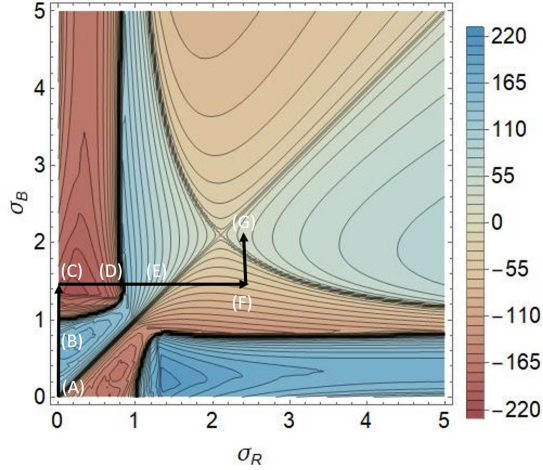


Figure 16.: A phase plot of combat outcomes with a labelled path. $\zeta_{BR} = \zeta_{RB} = 1.25$.

a larger phase advantage whilst the manoeuvre benefits begin to plateau. Once $\sigma_B > 1$, Red begins to achieve victory in engagements.

- Point (C) with $(\sigma_R, \sigma_B) = (0, 1.5)$: σ_B is large enough that the Blue network no longer decouples, and Red only receives resource and a higher local order parameter sporadically when combat nodes happen to coincide. However, this is more than sufficient to overcome the initial boost in Blue's superiority in resource transfer. Additionally, given Blue is only synchronised to a small extent, the local order parameter is often suboptimal as the non-engagement nodes frequency synchronise in a lagged position. Conversely, although Red spends a significant time with an even lower local order parameter between engagement and manoeuvre nodes, this nevertheless results in devastating losses for Blue.
- Path (C-D): A slight increase in Red internal coupling allows the Red non-combat nodes to group up, facilitating a faster Red manoeuvre when they happen to phase align with Red combat nodes. With the most optimal region of Red combat results being the domain around point (D).
- Path (D-E): As σ_R increases, Red begins to sacrifice its favourable engagement outcomes, with the critical transition occurring around $\sigma_R \approx 0.8$, when its engagement and manoeuvre nodes no longer periodically decouple. Past this value, both Blue and Red reach steady group frequencies rather than periodic decoupling behaviour. Notably, the increased Blue manoeuvre and local order parameter afforded by its larger internal coupling dominates the now reduced Red phase advantage.
- Path (E-F): Once σ_R crosses the neutral phase advantage line $\sigma_R = \sigma_B$, its larger intra-network coupling allows it to achieve victory over Blue. At this point both networks are receiving diminishing return on manoeuvre benefits and so the optimisation is between local order parameter between internal nodes and phase advantage over the opposition's engagement nodes.
- Path (F-G): Increasing σ_B to Point (G) $(\sigma_R, \sigma_B) = (2.5, 2.1)$ allows Blue to gain a phase advantage over Red which provides a slight advantage that grows over the course of the engagement.

In summary, intra and inter-network coupling work to divide the landscape into a number of regions according to whether internal coupling is large enough to overcome

the tension between engagement and manoeuvre nodes imposed by the value of ζ .

References

- Acebrón, J., Bonilla, L., Pérez-Vicente, C., Ritort, F., & Spigler, R. (2005) The Kuramoto model: a simple paradigm for synchronization phenomena. *Reviews of Modern Physics* **77**:137–83.
- Adams, E., & Mesterton-Gibbons, M. (2003) Lanchester’s attrition models and fights among social animals. *Behavioral Ecology* **14**(5):719–23.
- Alberts, D., Garstka, J., & Stein, F. (1999) *Network Centric Warfare*. (Command and Control Research Program, Washington DC).
- Arenas, A., Díaz-Guilera, A., Kurths, J., Moreno, Y., & Zhou, C. (2008) Synchronization in complex networks. *Physics Reports* **469**(3):93–153.
- Boccaletti, S., Bianconi, G., Criado, R., del Genio, C., Gómez-Gardeñes, J., Romance, M., Sendiña-Nadal, I., Wang, Z., & Zanin, M. (2014) The structure and dynamics of multi-layer networks *Physics Reports* **544**(1):1–122.
- Bollobás, B. (2013) *Modern Graph Theory* (Springer Science and Business Media, Berlin)
- Bracken, J. (1995) Lanchester models of the Ardennes campaign. *Naval Research Logistics* **42**(4):559–77.
- Deitchman, S. (1962) A Lanchester Model of Guerrilla Warfare. *Operations Research* **10**(6):818–27.
- Demazy, A., Kalloniatis, A., & Alpcan, T. (2018) A Game Theoretic Analysis of the Boyd-Kuramoto model. In: *9th GameSec — Decision and Game Theory for Security. Seattle USA October 29–31* Springer Proceedings **11199** p.248–64.
- Dörfler, F. & Bullo, F. (2014) Synchronization in complex networks of phase oscillators: a survey. *Automatica* **50**(6):1539–64.
- Fricker, R. (1998) Attrition models of the Ardennes campaign. *Naval Research Logistics* **45**(1):1–22.
- Holder, A., Zuparic, M., & Kalloniatis, A. (2017) Gaussian noise and the two-network frustrated Kuramoto model. *Physica D* **341**:10–32.
- Hollenbeck, J., & Spitzmueller, M. (2012) Team-structure: Tight versus Loose coupling in task-oriented groups. In: *Kozlowski, S. (editor) The Oxford Handbook of Organizational Psychology Vol 2*. Oxford University Press: p.733–66.
- Hughes, W. (1995) A salvo model of warships in missile combat used to evaluate their staying power. *Naval Research Logistics* **42**(2):267–89.
- Kalloniatis, A., Hoek, K., Zuparic, M., & Brede, M. (2020a) Optimising structure in a networked Lanchester model for fires and manoeuvre in warfare. *Journal of the Operational Research Society*. DOI: 10.1080/01605682.2020.1745701.
- Kalloniatis, A., McLennan-Smith, T., & Roberts, D. (2020b) Modelling distributed decision making in Command and Control using stochastic network synchronisation. *European Journal of Operational Research* **284** (2020) 588-603.
- Kalloniatis, A. & Zuparic, M. (2016) Fixed points and stability in the two-network frustrated Kuramoto model. *Physica A* **447**:21–35.
- Kress, M., Lin, K., & MacKay, NJ. (2018) The attrition dynamics of multilateral aar, *Operations Research* **66**(4), 950-956
- Kuramoto, Y. (1984) *Chemical oscillations, Waves, and Turbulence*. (Springer, Berlin).
- Lanchester, F. (1916) *Aircraft in warfare: The dawn of the fourth arm*. (Constable limited, London).
- Liu, J., Zhao, D., & Wang, F. (2013) Network attacks-defense model based on the improved Lanchester equation. *Proceedings of the 2013 International Conference on Machine Learning and Cybernetics*, Tianjin, 14–17 July.

- Lucas, T., & Turkes, T. (2004) Fitting Lanchester equations to the battles of Kursk and Ardennes. *Naval Research Logistics* **51**(1):95–116.
- MacKay, N. (2009) Lanchester models for mixed forces with semi-dynamical target allocation. *Journal of the Operational Research Society* **60**(10):1421–7.
- McLemore, C., Gaver, D., & Jacobs, P. (2016) A model for geographically distributed combat interactions of swarming naval and air forces. *Naval Research Logistics* **63**(7):562–576.
- Morse, P., Kimball, G., & Gass, S. (2003) *Methods in Operations Research* (Courier Corporation, Massachusetts)
- Neisser, U. (1976) *Cognition and Reality: Principles and Implications of Cognitive Psychology*. (Freeman: San Francisco).
- O’Keefe, K., & Bettstetter, C. (2019) A review of swarmalators and their potential in bio-inspired computing. arXiv:1903.11561
- Osinga, F. (2006) *Science, Strategy and War: The Strategic Theory of John Boyd (Strategy and History)*. (Routledge: London).
- Pecora, L., & Carroll, T. (1998) Master stability functions for synchronized coupled systems. *Physical Review Letters* **80**(10):2109
- Perrow, C. (2011) *Normal Accidents: Living with High Risk Technologies (Updated Edition)* (Princeton university Press, New Jersey)
- Plowes, N., & Adams, E. (2005) An empirical test of Lanchester’s square law: mortality during battles of the fire ant *Solenopsis invicta*. *Proceedings of the Royal Society B: Biological Sciences* **272**(1574):1809–14.
- Polybius, (1927) *The Histories*. (Harvard University Press, Cambridge).
- Reid, P. (2007) *A Brief History of Medieval Warfare: The Rise and Fall of English Supremacy at Arms, 1314–1485*. (Running Press, Philadelphia).
- Roberson, B. (2006) The colonel blotto game. *Economic Theory* **29**(1):1–24.
- Rodrigues, F., Peron, T., Ji, P., & Kurths, J. (2016) The Kuramoto model in complex networks. *Physics Reports* **610**:1–98.
- Sakaguchi, H., & Kuramoto, Y. (1986) A soluble active rotator model showing phase transitions via mutual entrainment. *Progress in Theoretical Physics* **76**(6):576–81.
- Schaffer, M. (1968) Lanchester Models of Guerrilla Engagements. *Operations Research* **16**(3):457–88.
- Stanescu, M., Barriga, N., & Buro, M. (2015) Using Lanchester attrition laws for combat prediction in StarCraft. *Eleventh Artificial Intelligence and Interactive Digital Entertainment Conference*.
- Van Creveld, M. (1985) *Command In War*. (Harvard University Press, Cambridge).
- Weick, K. (1976) Educational organizations as loosely coupled systems. *Administrative science quarterly* **21**(1):1–19.
- Zuparic, M., Angelova, M., Zhu, Y., & Kalloniatis, A. (2021) Adversarial decision strategies in multiple network phased oscillators: the Blue-Green-Red Kuramoto-Sakaguchi model. *Communications in Nonlinear Science and Numerical Simulation* **95**:105642.